Selective Assembly of Na,K-ATPase $\alpha_2\beta_2$ Heterodimers in the Heart
DISTINCT FUNCTIONAL PROPERTIES AND ISOFORM-SELECTIVE INHIBITORS*

Michael Habeck[‡], **Elmira Tokhtaeva**[§], **Yotam Nadav**[‡], **Efrat Ben Zeev**[¶], **Sean P. Ferris**[‖1], **Randal J. Kaufman**[‖2], **Elizabeta Bab-Dinitz**[‡], **Jack H. Kaplan**[**], **Laura A. Dada**[‡‡], **Zvi Farfel**[‡§§], **Daniel M. Tal**[‡], **Adriana Katz**[‡], **George Sachs**[§], **Olga Vagin**[§3], and **Steven J. D. Karlish**[‡4]

From the [‡]Department of Biomolecular Sciences and [¶]Israel National Centre for Personalized Medicine, Weizmann Institute of Science, Rehovoth 7610001, Israel, the [§§]School of Medicine, Tel Aviv University, Tel Aviv 6997801, Israel, the [§]Department of Physiology, School of Medicine, UCLA and Veterans Affairs Greater Los Angeles Healthcare System, Los Angeles, California 90073, the [‖]Department of Biological Chemistry, University of Michigan Medical Center, Ann Arbor, Michigan 48109, the [**]Department of Biochemistry and Molecular Genetics, University of Illinois, Chicago, Illinois 60607, and the [‡‡]Division of Pulmonary and Critical Care Medicine, Feinberg School of Medicine, Northwestern University, Chicago, Illinois 60611

The Na,K-ATPase α_2 subunit plays a key role in cardiac muscle contraction by regulating intracellular Ca^{2+}, whereas α_1 has a more conventional role of maintaining ion homeostasis. The β subunit differentially regulates maturation, trafficking, and activity of α-β heterodimers. It is not known whether the distinct role of α_2 in the heart is related to selective assembly with a particular one of the three β isoforms. We show here by immunofluorescence and co-immunoprecipitation that α_2 is preferentially expressed with β_2 in T-tubules of cardiac myocytes, forming $\alpha_2\beta_2$ heterodimers. We have expressed human $\alpha_1\beta_1$, $\alpha_2\beta_1$, $\alpha_2\beta_2$, and $\alpha_2\beta_3$ in *Pichia pastoris*, purified the complexes, and compared their functional properties. $\alpha_2\beta_2$ and $\alpha_2\beta_3$ differ significantly from both $\alpha_2\beta_1$ and $\alpha_1\beta_1$ in having a higher $K_{0.5}K^+$ and lower $K_{0.5}Na^+$ for activating Na,K-ATPase. These features are the result of a large reduction in binding affinity for extracellular K^+ and shift of the E_1P-E_2P conformational equilibrium toward E_1P. A screen of perhydro-1,4-oxazepine derivatives of digoxin identified several derivatives (*e.g.* cyclobutyl) with strongly increased selectivity for inhibition of $\alpha_2\beta_2$ and $\alpha_2\beta_3$ over $\alpha_1\beta_1$ (range 22–33-fold). Molecular modeling suggests a possible basis for isoform selectivity. The preferential assembly, specific T-tubular localization, and low K^+ affinity of $\alpha_2\beta_2$ could allow an acute response to raised ambient K^+ concentrations in physiological conditions and explain the importance of $\alpha_2\beta_2$ for cardiac muscle contractility. The high sensitivity of $\alpha_2\beta_2$ to digoxin derivatives explains beneficial effects of cardiac glycosides for treatment of heart failure and potential of $\alpha_2\beta_2$-selective digoxin derivatives for reducing cardiotoxicity.

The Na,K-ATPase plays a key role in cardiac muscle contractility by regulating the cytosolic Ca^{2+} concentration, via the Na^+/Ca^{2+} exchanger, and hence the excitation-contraction coupling in cardiac myocytes (1). Three isoforms of the Na,K-ATPase α subunit and three isoforms of the β subunit are expressed in cardiac muscle, and their expression levels vary between species (2–4). In addition, the regulatory FXYD1 subunit and possibly other FXYD proteins are expressed in cardiac muscle (5, 6). Although α_1 is the most abundant α subunit isoform in cardiomyocytes in the majority of species, the α_2 isoform is functionally more important for cardiac muscle contractility (7–11). The mechanisms underlying distinct roles of α_2 and α_1 isoforms in the heart are unclear. In smooth and skeletal muscle, the α_2 subunit is concentrated at the junctions between the tubular membrane and sarcoplasmic reticulum in close proximity to the Na^+/Ca^{2+} exchanger and other components of the excitation-contraction complex (12), resulting in more efficient regulation of contraction by the α_2 subunit in contrast to uniformly distributed α_1 subunit. However, the published data on localization of the two isoforms in cardiac myocytes is inconsistent. For example, preferential T-tubular localization of α_2 but uniform plasma membrane localization of the α_1 have been reported by several groups (11, 13), whereas quite the opposite distribution of the isoforms was reported (3), and uniform distribution of both α_1 and α_2 subunits has also been reported (14). Measurements of the Na,K-ATPase function of isoforms in cardiac myocytes suggest that the α_2 subunit is more concentrated in T-tubular membranes than in the external sarcolemma, whereas the α_1 subunit is equally distributed in the plasma membrane (11, 15, 16).

Assembly with the β subunit is required for maturation, trafficking, membrane insertion, and transport activity of the α subunit (17), and three β isoforms differentially regulate these processes. Three β subunit isoforms differ from each other in

[1] Present address: Dept. of Pathology, University of California, 513 Parnassus Ave., Health Sciences West 451, Box 0102, San Francisco, CA 94143.
[2] Present address: Rm. 7103, Sanford-Burnham-Prebys Medical Discovery Institute, 10901 N. Torrey Pines Rd., La Jolla, CA 92037.
[3] To whom correspondence may be addressed: Dept. of Physiology, School of Medicine, UCLA and Veterans Administration Greater Los Angeles Health Care System, Los Angeles, California, CA. Tel.: 310-478-3711 (ext. 42055); Fax: 310-312-9478; E-mail: olgav@ucla.edu.
[4] To whom correspondence may be addressed: Dept. of Biomolecular Sciences, Weizmann Institute of Science, Rehovot, 7610001, Israel. Tel.: 972-8-934-2278; Fax: 972-8-934-4118; E-mail: Steven.Karlish@weizmann.ac.il.

the number of N-linked glycans, and recombinant addition or removal of N-glycans has been shown to alter the polarized sorting of the Na,K-ATPase (18, 19). The three β subunit isoforms differentially modulate voltage dependence of the Na,K-ATPase activity and the apparent affinity of the enzyme for Na$^+$, K$^+$ and inhibitors (20, 21). β_1, but not β_2 or β_3, undergoes post-translational modifications, namely glutathionylation and palmitoylation, and β_1 glutathionylation induced by oxidants decreases the Na,K-ATPase activity (22, 23). Thus, the specific assembly with particular β isoforms could account for distinct physiological roles of α_1 and α_2 isoforms. However, it is not known whether the α_2 subunit has a preference for a particular β isoform in cardiac myocytes.

To examine possible functional differences between $\alpha_2\beta_{(1–3)}$ isoforms, we have expressed human α_2 with all three human β subunits in *Pichia pastoris,* purified the complexes, and compared their functional characteristics and inhibitor sensitivity. Previous work has demonstrated some features of $\alpha_2\beta_2$ and $\alpha_2\beta_3$ when expressed in *Xenopus* oocytes and SF-9 insect cells (20, 24). Experimentally, the purified complexes are advantageous in that they allow characterization of the functional properties and inhibitor selectivity of each isoform separately (25–27) and also detailed mechanistic properties of ion binding and conformational changes (28–30).

The inhibition of the Na,K-ATPase by digitalis CGs[5] has been used for years to treat heart failure. CGs increase the force of cardiac muscle contraction by reducing the inward Na$^+$ gradient that decreases Ca^{2+} extrusion via the Na$^+$/Ca^{2+} exchanger (NCX1), leading to increased Ca^{2+}-induced Ca^{2+} release from the sarcoplasmic reticulum during excitation-contraction coupling. As a toxic side effect, excessive inhibition of the Na,K-ATPase increases bulk intracellular Na$^+$ concentration, excessive accumulation of Ca^{2+} ions (*i.e.* "calcium overload"), and "spontaneous" Ca^{2+} release from sarcoplasmic reticulum that can trigger cardiac arrhythmias (1, 31). The preferential role of α_2 in excitation-contraction coupling suggests that α_2-specific inhibitors might be able to induce an ionotropic effect without triggering Ca^{2+} overload and arrhythmias. Some years ago, we demonstrated that some natural CGs, such as digoxin and digitoxin, exhibit a moderate intrinsic selectivity for α_2 over α_1, whereas aglycones, such as digoxigenin and digitoxigenin, show no selectivity (25). Thus, the isoform selectivity was attributed to the sugar moiety, especially the third digitoxose. It was proposed that modification of the third sugar could raise selectivity for α_2. Indeed, chemical modification of the third digitoxose residue of digoxin by periodate oxidation and reductive amination by primary amines, R-NH$_2$, produced perhydro-1,4-oxazepine derivatives with enhanced selectivity

of inhibition for $\alpha_2\beta_1$ over $\alpha_1\beta_1$ (27). Most recently, we have described perhydro-1,4-oxazepine digoxin derivatives with various straight chain, branched, and cyclic or heterocyclic aliphatic substitutions and shown that compounds with four carbon substitutions (cyclobutyl (DcB), methyl cyclopropyl (DMcP), and isobutyl (DiB)) showed an especially high selectivity for $\alpha_2\beta_3/\alpha_1\beta_1$. $\alpha_2\beta_3$ is the principal Na,K-pump isoform in non-pigmented cells of ciliary epithelium. We have shown that the digoxin derivatives with enhanced selectivity for $\alpha_2\beta_1$ and especially $\alpha_2\beta_3$ efficiently reduce intraocular pressure when applied topically to rabbit eyes (26, 27).

We present evidence here that the α_2 and β_2 isoforms preferentially assemble with each other in the heart and reside predominantly in the T-tubules. By systematic analysis of properties of purified $\alpha_2\beta_2$ in comparison with $\alpha_1\beta_1$, $\alpha_2\beta_1$, and $\alpha_2\beta_3$, we demonstrate distinctive functional properties and isoform-selective inhibition of $\alpha_2\beta_2$, which explain the important role of α_2 for myocardial contractility and the pharmacological potential of $\alpha_2\beta_2$-selective CGs.

Results

Distribution of Na,K-ATPase α_1, α_2, β_1, and β_2 Subunits in Rat and Human Heart—Normal rat or human frozen heart sections were used to study the intracellular localization of the Na,K-ATPase subunit isoforms by immunofluorescence. In rat cardiomyocytes, the Na,K-ATPase subunits were differentially distributed (Fig. 1A). The α_1 isoform was less abundant in the T-tubular membranes than in the external sarcolemma. Conversely, the α_2 isoform was more abundant in the T-tubular membranes than in the sarcolemma, consistent with previously published results (11, 13, 21). Both isoforms are expressed at the intercalated discs, but α_1 subunit expression is more pronounced. The immunofluorescence pattern with the Na,K-ATPase β_2 antibody was similar to that of the α_2 antibody with major expression observed in the T-tubules. In frozen sections of human hearts, the β_1 isoform was present more abundantly in the sarcolemma than in the T-tubular membranes, whereas the β_2 isoform was present exclusively in the T-tubules (Fig. 1B). These results demonstrate a differential localization of the Na,K-ATPase subunits with the α_2 and β_2 Na,K-ATPase subunits following the same T-tubule-specific expression pattern and the α_1 and the β_1 subunits ubiquitously distributed but more abundant in the sarcolemma.

Because the Na,K-ATPase is a crucial component in regulating postnatal cardiac function (32), we analyzed whether the Na,K-ATPase subunits are also selectively expressed during embryogenesis. Paraffin-embedded sections of mouse embryos (embryonic day 12.5) were analyzed by immunofluorescence (Fig. 2). The Na,K-ATPase α_1 subunit was expressed ubiquitously (*top* and *bottom left panels*), whereas the α_2 and β_2 were mostly restricted to the heart (*top* and *bottom right panels*, respectively).

The Na,K-ATPase α_2 and β_2 Subunits Are Selectively Co-immunoprecipitated from Mouse Heart—To analyze the composition of the Na,K-ATPase heterodimers present in heart microsomal membranes, proteins were co-immunoprecipitated with an α_2 subunit-specific antibody, and the presence of α_1, β_1, β_2, and β_3 subunits was analyzed by Western blotting.

---

[5] The abbreviations used are: CG, cardiac glycoside; NCX1, Na/Ca exchanger isoform 1; C$_{12}$E$_8$, octaethylene glycol monodecyl ether; PNGase F, peptide: N-glycosidase F; RH421, N-(4-sulfobutyl)-4-(4-(4-(dipentylamino)phenyl) butadienyl)pyridinium; SOPS, 1-stearoyl-2-oleoyl-*sn*-glycero-3-phospho-L-serine; DMe, methylamine; DEt, ethylamine; DP, propylamine; DiP, isopropylamine; DcP, cyclopropylamine; DiB, isobutylamine; DMcP, methyl-cyclo-propylamine; DcB, cyclobutylamine; DAz, azetidine-3-amine; DTh, thietane-3-amine; DcPe, cyclopentylamine; DcHe, cyclohexylamine; DcB2,2dM, 2,2-dimethylcyclobutylamine; DMcB3,3dM, methylcyclobutyl-amine-3,3-dimethyl; DMSM, (2-methylsulfonyl)methylamine; DEMS, (2-ethylsulfonyl)methylamine; DESA, (2-sulfonamide)ethylamine.
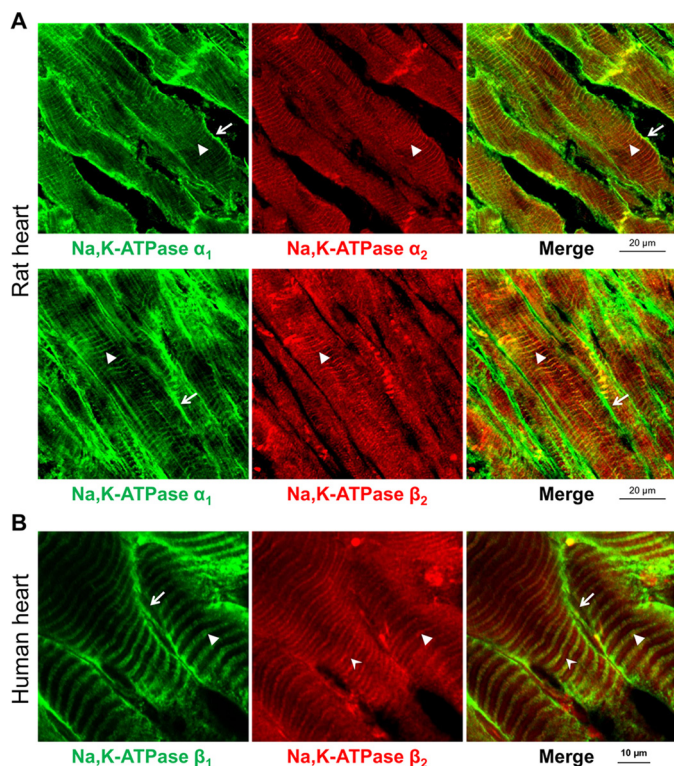
FIGURE 1. **Na,K-ATPase β_2 and α_2 subunits are localized almost exclusively in T-tubules in cardiomyocytes, whereas the α_1 and β_1 subunits are localized in both sarcolemma and T-tubules.** *A*, frozen sections of rat heart were double-stained by using mouse antibodies against α_1 subunit (*green*) and rabbit antibodies against α_2 subunit (*red*) (*top panels*) or by using mouse antibodies against α_1 subunit (*green*) and rabbit antibodies against β_2 subunit (*red*) (*bottom panels*). Anti-mouse Alexa Fluor 488-conjugated secondary antibodies were used to detect anti-α_1 primary antibodies, and anti-rabbit Alexa Fluor 633-conjugated secondary antibodies were used to detect anti-β_2 and anti-α_2 primary antibodies. The *arrows* show localization of the α_1 subunits, but not of α_2 and β_2 subunits, in the sarcolemma. The *arrowheads* show co-localization of α_1 and β_2 subunits or α_1 and α_2 subunits in T-tubules. *B*, frozen sections of human heart were double-stained by using mouse antibodies against β_1 subunit (*green*) and rabbit antibodies against β_2 subunit (*red*). Anti-mouse Alexa Fluor 488-conjugated secondary antibodies were used to detect anti-β_1 primary antibodies, and anti-rabbit Alexa Fluor 633-conjugated secondary antibodies were used to detect anti-β_2 primary antibodies. The *arrows* show localization of the β_1 subunits, but not of β_2 subunits, in the sarcolemma. The *arrowheads* show co-localization of β_1 and β_2 subunits in T-tubules. The *stealth-like arrowheads* show the T-tubules in which the β_2 subunits, but not the β_1 subunits, are present.

To prevent the overlap of the β subunits bands with the band corresponding to the heavy chain of the immunoprecipitating antibody, the immunoprecipitated proteins were treated with PNGase F before SDS-PAGE. Immunoprecipitation of the α_2 subunit resulted in the co-immunoprecipitation of the β_2 subunit and minor amounts of β_1 and β_3 subunits (Fig. 3*A*, *left*). No α_1 subunits were detected in the immunoprecipitation with the α_2-specific antibody. In contrast, when the α isoform-nonspecific antibody was used, both α_1 and α_2 subunits were immunoprecipitated, and approximately equal amounts of all of the three β subunits were co-immunoprecipitated (Fig. 3*A*, *right*). Conversely, immunoprecipitation with a β_2-specific antibody resulted in co-immunoprecipitation of the α_2 but not the α_1 subunit (Fig. 3*B*). Taken together, these results suggest that the α_2 and β_2 subunit isoforms associate predominantly with each other but not with other isoforms expressed in the heart.

Expression and Purification of Na,K-ATPase $\alpha_2\beta_2$—$\alpha_2\beta_2$ and $\alpha_2\beta_3$ were expressed in *P. pastoris* as described under "Experimental Procedures." Under optimal expression conditions, specific ouabain binding for the $\alpha_2\beta_2$ clone was 8 ± 1 pmol/mg protein and 10 ± 2 pmol/mg for the $\alpha_2\beta_3$ clone, respectively. The addition of DMSO to the culture medium, which was reported to increase expression of GPCRs in *P. pastoris*, did not increase expression (33).

Both isoforms were purified via the N-terminal His tag of the β subunit by metal affinity chromatography on BD-Talon beads and reconstituted with purified human FXYD1 on the BD-Talon beads, as described in Experimental Procedures.[6] The purity of $\alpha_2\beta_2$ and $\alpha_2\beta_3$ was comparable with that of purified human $\alpha_1\beta_1$ and $\alpha_2\beta_1$ complexes. As depicted in Fig. 4, at least five bands of β_2 were observed, in comparison with two bands for β_3 and β_1. The two bands of β_1 were shown previously to represent two glycosylated versions of the β_1 subunit of the Man$_X$-GlcNAc$_2$ type, typical for *P. pastoris* (34). An increase in heterogeneity of glycoforms of β_2 as compared with β_3 and β_1 is consistent with the presence of eight *N*-glycosylation sites in β_2 and only two and three in β_3 and β_1, respectively. When deglycosylated by PNGase treatment, all three β isoforms migrated at their expected molecular mass of approximately 35, 31, and 33 kDa for β_1, β_3, and β_2, respectively.

Recent studies have demonstrated that $\alpha_2\beta_1$ is less stable to thermal and detergent-mediated inactivation than $\alpha_1\beta_1$, due to suboptimal interaction with phosphatidylserine (35). We investigated the relative effect of the β subunit on Na,K-ATPase isoform stability by thermal inactivation of [^{3}H]ouabain binding to the membranes and Na,K-ATPase activity of the purified proteins, as described in previous publications (see for example Refs. 29 and 65). By both criteria, the α_2 complexes were significantly less thermally stable than α_1, and $\alpha_2\beta_2$ was somewhat less stable than $\alpha_2\beta_1$ and $\alpha_2\beta_3$. Thus, the relative instability of the $\alpha_2\beta_{(1-3)}$ complexes is a feature attributable primarily to the α_2 subunit. The differences between β isoforms, $\beta_2 < \beta_3 \approx \beta_1$, are rather small.

Functional Properties of Purified $\alpha_1\beta_1$, $\alpha_2\beta_1$, $\alpha_2\beta_2$, and $\alpha_2\beta_3$ Complexes—The specific Na,K-ATPase activity of the purified isoforms was highest for $\alpha_1\beta_1$ (16.4 ± 0.7 μmol/mg/min), followed by similar values for $\alpha_2\beta_1$ (10.9 ± 0.6), $\alpha_2\beta_3$ (10.7 ± 1.9), and $\alpha_2\beta_2$ (8.4 ± 1.4; Table 1, column 2). Note that FXYD1 itself inhibits the Na,K-ATPase activity of the purified human $\alpha_1\beta_1$ by about 25% and $\alpha_2\beta_1$ by about 15% compared with the $\alpha\beta$ complexes alone (30). One kinetic property showing large differences between the isoform complexes was the $K_{0.5}K^+$ for activation of Na,K-ATPase activity, with values of 1.5 ± 0.1 mM for $\alpha_1\beta_1$ and 2.7 ± 0.1 mM for $\alpha_2\beta_1$, whereas the $K_{0.5}K^+$ for both $\alpha_2\beta_2$ and $\alpha_2\beta_3$ was much higher, with apparent $K_{0.5}$ values of 7.4 ± 0.2 and 6.4 ± 0.5 mM, respectively (Table 1, column 4). Sodium titrations for activation of Na,K-ATPase activity revealed that $K_{0.5}Na^+$ was not different between $\alpha_1\beta_1$ and $\alpha_2\beta_1$, whereas $K_{0.5}Na^+$ for $\alpha_2\beta_2$ and $\alpha_2\beta_3$ was significantly lower (Table 1, column 3). We have also looked at the affinity for

---

[6] All purified proteins described here are the $\alpha\beta$FXYD1 complexes, although, for simplicity, when referring to or naming the different isoform complexes, the FXYD1 has been omitted.
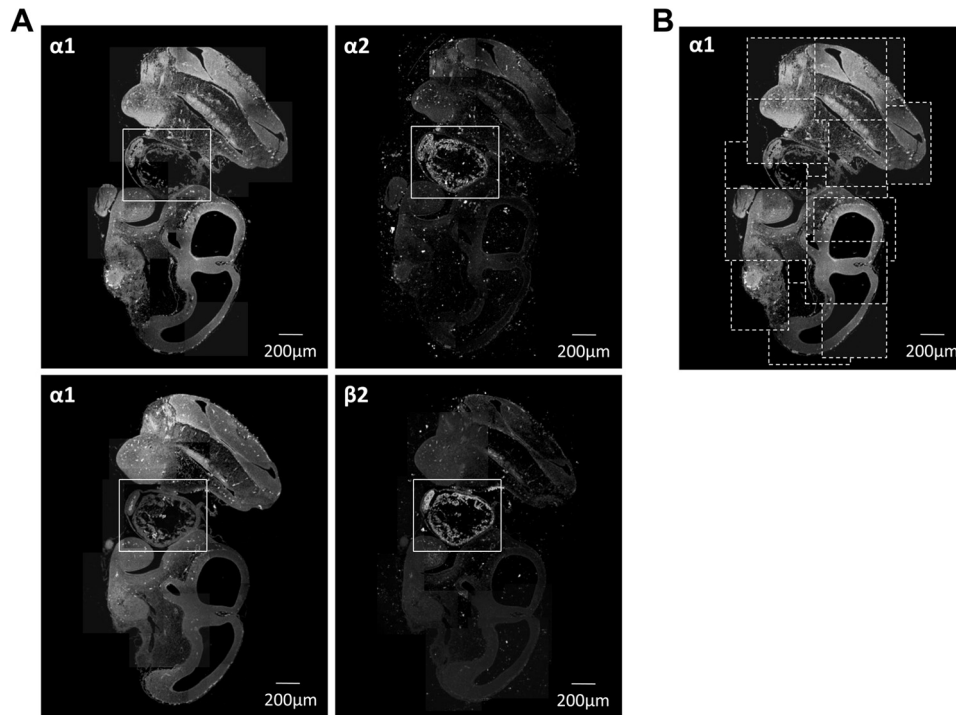
FIGURE 2. The Na,K-ATPase α_2 subunit and β_2 subunit are preferentially expressed in the mouse embryonic heart in contrast to the ubiquitously expressed α_1 subunit. *A*, paraffin-embedded sections of mouse embryos (embryonic day 12.5) were double-stained by using mouse antibodies against α_1 subunit (*left panels*) and rabbit antibodies against α_2 subunit or β_2 subunit (*right panels*). Anti-mouse Alexa Fluor 488-conjugated secondary antibodies were used to detect anti-α_1 primary antibodies, and anti-rabbit Alexa Fluor 633-conjugated secondary antibodies were used to detect anti-α_2 or anti-β_2 primary antibodies. The *rectangles* show the embryonic hearts. *B*, a scheme demonstrating the assembly of the images shown in *A*. Each *rectangle outlined* by a *dotted line* represents an individual confocal microscopy image taken at $\times10$ magnification.
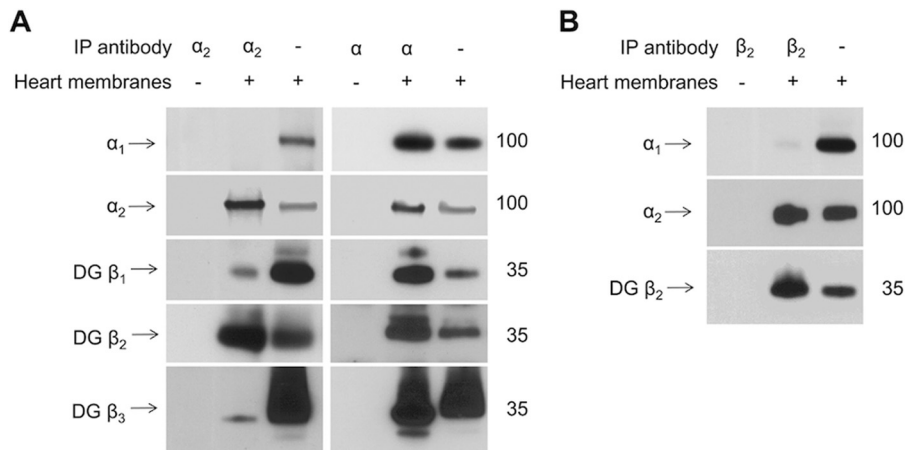

FIGURE 3. The Na,K-ATPase α_2 subunit and β_2 subunit preferentially interact with each other in mouse heart. *A*, Western blotting analysis of proteins immunoprecipitated and co-immunoprecipitated from the detergent extracts of mouse heart microsome membranes by using either the α_2-specific antibodies (*left panels*) or the α-nonspecific antibodies (*right panels*) shows preferential co-immunoprecipitation of the β_2 subunit with the α_2 subunit. *B*, Western blotting analysis of the immunoprecipitated β_2 subunit and co-immunoprecipitated α_2 subunit isoforms shows that the α_2 subunit is preferentially co-precipitated with the β_2 subunit. Input lanes contain 10% of the extract used for immunoprecipitation. To prevent an overlap of the β subunit bands with the heavy chain band of the antibodies used for immunoprecipitation, the immunoprecipitated proteins were treated with PNGase F before SDS-PAGE. *IP*, immunoprecipitation; *DG*, deglycosylated.

inhibition of Na,K-ATPase activity by vanadate, which is a phosphate analogue that binds to the $E_2(2K)$ conformation, mimicking the transition state E_2P2K during dephosphorylation (36). All three α_2 isoforms have a higher K_i vanadate compared with $\alpha_1\beta_1$ ($K_i = 0.48$ μM), and the effects are greatest with β_2 and β_3 in the order $\alpha_2\beta_2$ ($K_i = 34$ μM) > $\alpha_2\beta_3$ ($K_i = 19$ μM) > $\alpha_2\beta_1$ ($K_i = 3.5$ μM) (Table 1, column 5).

A simple explanation of the raised $K_{0.5}K^+$ in Na,K-ATPase activity assays could be that the β_2 and β_3 subunit reduce the

binding affinity of 2K ions for their extracellular sites. K^+ and Na^+ binding was determined by using the electrochromic shift dye RH421 in a medium of fixed ionic strength (containing also 5 mM magnesium ions) (Fig. 5 and Table 2) (29, 30, 37). The *inset* of Fig. 5A shows the typical RH421 responses upon the addition of Na^+ ions (E_1-E_1(3Na)) and then ATP (to E_2P) and K^+ ions ($E_2(2K)$) for the $\alpha_2\beta_2$ complex, as explained in recent papers (29). By varying Na^+ or K^+ concentrations, equilibrium titrations of either $3Na^+$ binding to cytoplasmic sites or $2K^+$
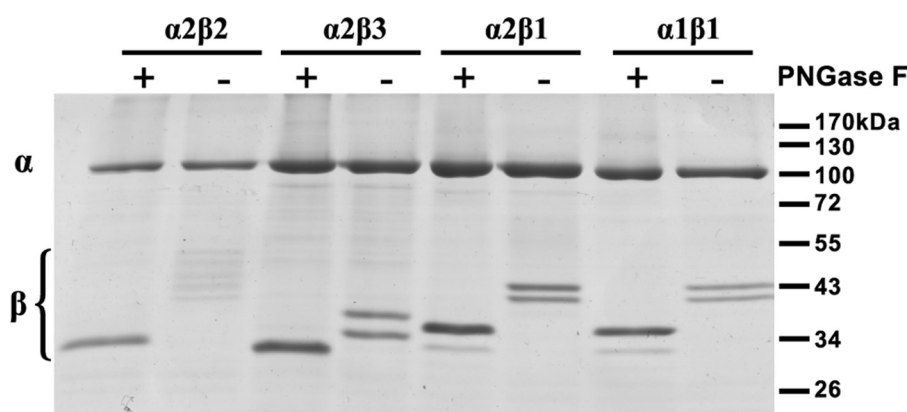
FIGURE 4. **Expression of purified Na,K-ATPase isoforms.** Coomassie-stained SDS-PAGE of purified isoforms (5 μg/lane). For deglycosylation, samples were denatured and treated with PNGase F for 60 min at 37 °C.

TABLE 1

Functional properties of purified Na,K-ATPase complexes

Specific activity, $K_{0.5}Na^+$, $K_{0.5}K^+$, and K_i vanadate of purified Na,K-ATPase complexes are shown. Values represent averages of at least three different experiments $\pm$ S.E. The reaction medium contained sodium plus potassium as indicated, 1 mM ATP, 3 mM MgCl$_2$, 25 mM histidine, pH 7.4, 1 mM EGTA, 0.01 mg/ml SOPS, 0.001 mg/ml cholesterol, and 0.005 mg/ml C$_{12}$E$_8$. Maximal Na,K-ATPase activity was measured in the presence of 120 mM NaCl, 20 mM KCl. For ion titrations, ATPase activity was measured in medium containing 80 mM KCl and 0–120 mM NaCl or 120 mM NaCl and 0–40 mM KCl. Ionic strength was maintained constant with choline chloride. $K_{0.5}$ values were obtained from least square fits of the data points to the Hill equation. K_i vanadate was determined in medium containing 120 mM NaCl, 20 mM KCl, and 1 mM ATP, and data points were fitted to a one-side inhibition model.

Isoform complexes	Specific Na,K-ATPase activity	$K_{0.5}Na^+$ (n_H)	$K_{0.5}K^+$ (n_H)	Vanadate K_i
	μmol/mg/min	*mM*	*mM*	*μM*
$\alpha_1\beta_1$	16.4 $\pm$ 0.7	16 $\pm$ 0.4 (1.7 $\pm$ 0.1)	1.5 $\pm$ 0.1 (1.8 $\pm$ 0.1)	0.5 $\pm$ 0.1
$\alpha_2\beta_1$	10.9 $\pm$ 0.6	17.7 $\pm$ 0.5 (1.9 $\pm$ 0.2)	2.7 $\pm$ 0.1 (2.0 $\pm$ 0.2)	3.5 $\pm$ 0.3
$\alpha_2\beta_2$	8.4 $\pm$ 1.4	9.8 $\pm$ 0.7 (1.8 $\pm$ 0.2)	7.4 $\pm$ 0.2 (1.7 $\pm$ 0.1)	34.0 $\pm$ 2.0
$\alpha_2\beta_3$	10.7 $\pm$ 1.9	13.0 $\pm$ 0.2 (1.9 $\pm$ 0.2)	6.4 $\pm$ 0.5 (1.8 $\pm$ 0.2)	19.0 $\pm$ 1.5

binding to extracellular sites are readily obtained, leading to curves such as those in Fig. 5, *A* and *B*. The binding parameters derived from best fits of the curves to the Hill equation are collected in Table 2, where $K_{0.5}Na^+$ and $K_{0.5}K^+$ represent the intrinsic binding affinity for 3Na$^+$ and 2K$^+$ ions, respectively. Evidently, the intrinsic binding affinity for 3Na$^+$ ions is the same for all of the isoform complexes. By contrast, in these conditions, the binding affinity of 2K$^+$ ions to $\alpha_2\beta_1$ is significantly lower than to $\alpha_1\beta_1$, and the binding affinity for both $\alpha_2\beta_2$ and $\alpha_2\beta_3$ is further strongly reduced compared with $\alpha_2\beta_1$. Note that, compared with $K_{0.5}K^+$ for $\alpha_1\beta_1$, the $K_{0.5}K^+$ for $\alpha_2\beta_2$ or $\alpha_2\beta_3$ is almost an order of magnitude higher. Because vanadate binds primarily to the E$_2$(2K) conformation, the differences in K_i for vanadate inhibition of Na,K-ATPase activity could be secondary to the differences in $K_{0.5}K^+$ values, with the same order for the K_i as for $K_{0.5}K^+$ values ($\alpha_1\beta_1 < \alpha_2\beta_1 < \alpha_2\beta_3 < \alpha_2\beta_2$; Table 1).

An alternative or additional explanation to that just given is that raised $K_{0.5}K^+$ of the $\alpha_2\beta_2$ and $\alpha_2\beta_3$ complexes is caused by an $\alpha_2\beta_2$- or $\alpha_2\beta_3$-induced shift in poise of the E$_1$-E$_2$ conformational equilibrium toward E$_1$ or E$_1$-P. This explanation would also be consistent with the parallel reduction in apparent $K_{0.5}Na^+$ and increase in K_i for vanadate (Table 1, column 3). A direct test of the relative effects of β_1, β_2, and β_3 on the conformational changes was made by measuring the rates of the E$_1$P(3Na) $\rightarrow$ E$_2$P and E$_2$(2Rb)ATP $\rightarrow$ E$_1$3Na·ATP transitions using RH421 in stopped-flow experiments, as described in our recent publications (29, 30). Traces for the $\alpha_2\beta_2$ complex are shown in Fig. 5, *C* and *D*, and the rate constants for all of the isoform complexes are collected in Table 3. These data show

directly that for $\alpha_2\beta_1$, the rates of E$_1$P(3Na) $\rightarrow$ E$_2$P are indeed slower than for $\alpha_1\beta_1$, and for both $\alpha_2\beta_2$ and $\alpha_2\beta_3$, the rate is still slower than for $\alpha_2\beta_1$.

The rates of E$_2$(2Rb)ATP $\rightarrow$ E$_1$3Na·ATP for $\alpha_2\beta_1$, $\alpha_2\beta_2$, and $\alpha_2\beta_3$ are all significantly slower than for $\alpha_1\beta_1$, but they are indistinguishable from each other. The turnover rate in s^{-1} for each isoform was calculated from the expression $(a \times b)/(a + b)$, where a is the rate of E$_1$P(3Na) $\rightarrow$ E$_2$P and b is the rate of E$_2$(2Rb)ATP $\rightarrow$ E$_1$3Na·ATP (Table 3), assuming that the rates of phosphorylation E$_1$Na + ATP $\rightarrow$ E$_1$P(3Na) and dephosphorylation E$_2$P2Rb $\rightarrow$ E$_2$(2Rb) are fast and do not significantly limit the turnover rate. The calculated value for $\alpha_1\beta_1$ (14 s^{-1}) is greater than for $\alpha_2\beta_1$, $\alpha_2\beta_2$, and $\alpha_2\beta_3$, which are not significantly different from each other (9.17, 8.76, and 8.75 s^{-1}, respectively; average of 8.89). The ratios of the calculated turnover rates for $\alpha_1\beta_1/\alpha_2\beta_1$, $\alpha_1\beta_1/\alpha_2\beta_2$, and $\alpha_1\beta_1/\alpha_2\beta_3$ are essentially the same, with an average of 1.6. These ratios are close to those of Na,K-ATPase activities in Table 1, validating the assumptions that underlie the calculation of the turnover rates.

Inhibition of Na,K-ATPase Isoforms by Perhydro-1,4-oxazepine Derivatives of Digoxin—As reported recently, chemical modification of the third digitoxose residue of digoxin (by periodate oxidation and reductive amination with R-NH$_2$) to produce perhydro-1,4-oxazepine derivatives increases selectivity of inhibition for $\alpha_2\beta_1$ and $\alpha_2\beta_3$ over $\alpha_1\beta_1$ (26, 27). Here we have compared inhibition of $\alpha_1\beta_1$ and all three complexes $\alpha_2\beta_1$, $\alpha_2\beta_2$, and $\alpha_2\beta_3$ by several derivatives described previously (26) and six new ones (DAz, DTh, DcB2,2dM, DMSM, DEMS, and DESA). The structures of the substituents, abbreviated names, and masses of all of the derivatives are given in Fig. 6. Fitted K_i
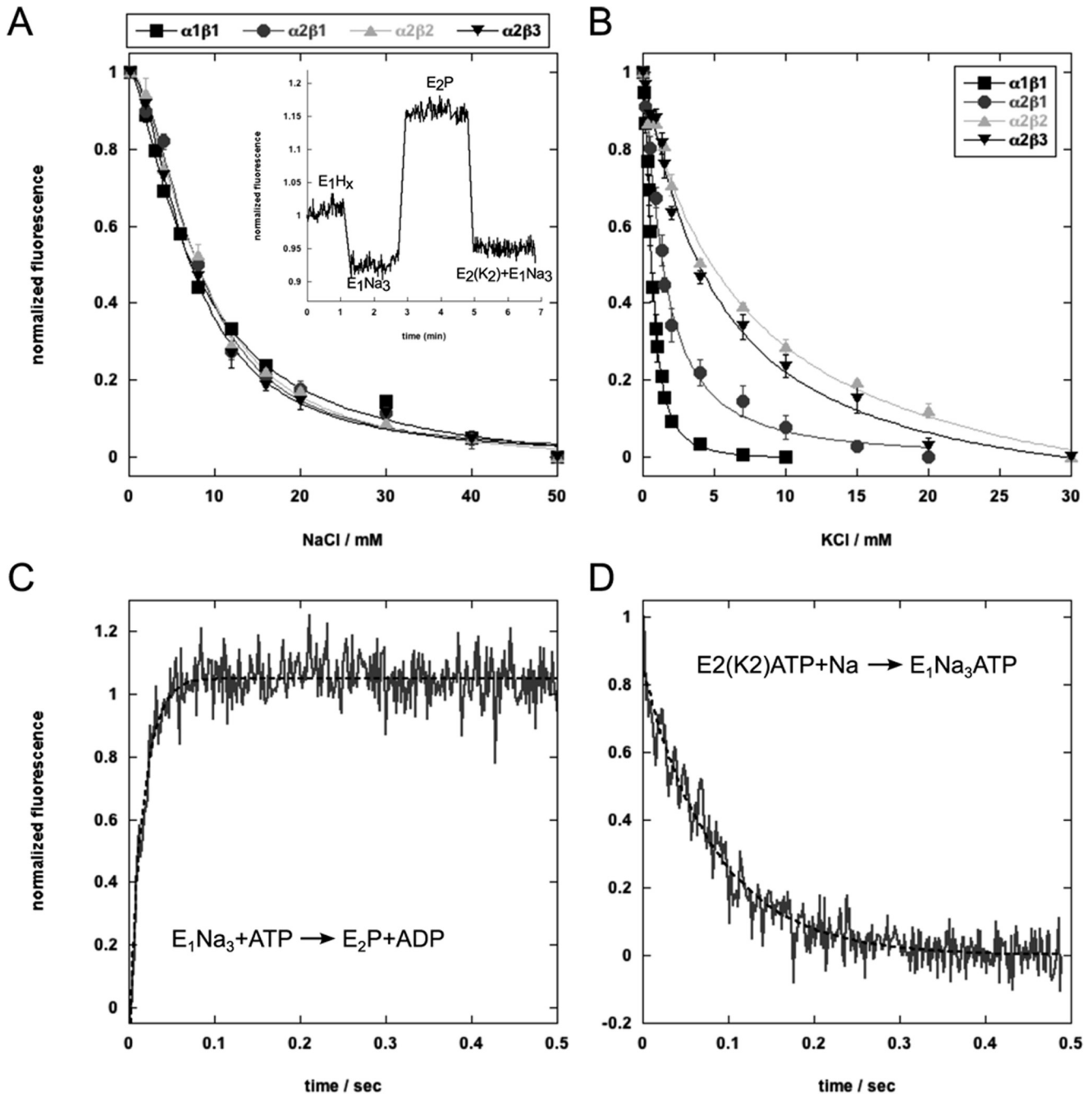
FIGURE 5. **Sodium and potassium binding and conformational changes of the isoforms measured with RH421.** *A*, equilibrium titration of sodium binding to the E_1 conformation. The *inset* shows a standard experiment and fluorescence changes associated with ion binding and release to $\alpha_2\beta_2$ (sodium binding to E_1, sodium release and conformational transition to E_2P, and potassium binding). *B*, equilibrium titration of potassium binding to E_2P. *C*, stopped-flow trace of the $E_1Na3 \rightarrow E_2P$ transition of $\alpha_2\beta_2$ fitted to a double exponential function. The average of 15 traces is shown. *D*, stopped-flow trace of the $\alpha_2\beta_2$ $E_2(Rb2)ATP \rightarrow E_1Na3ATP$ transition fitted to a single exponential function.

TABLE 2

Binding affinities of sodium and potassium detected with RH421

Sodium or potassium titration curves in Fig. 5 were fitted to the Hill equation. The $K_{0.5}$ and n_H values represent averages from three experiments ±S.E.

Isoform	$K_{0.5}Na^+$ (n_H)	$K_{0.5}K^+$ (n_H)
	mM	*mM*
$\alpha_1\beta_1$	7.7 ± 0.5 (1.7 ± 0.13)	0.6 ± 0.04 (1.8 ± 0.1)
$\alpha_2\beta_1$	8.0 ± 0.3 (1.9 ± 0.2)	1.5 ± 0.1 (1.5 ± 0.1)
$\alpha_2\beta_2$	8.1 ± 0.3 (1.7 ± 0.2)	5.1 ± 0.1 (1.6 ± 0.1)
$\alpha_2\beta_3$	7.3 ± 0.6 (1.8 ± 0.1)	4.8 ± 0.6 (1.5 ± 0.2)

values and selectivity ratios for all of these compounds are summarized in Table 4. Compounds that have the highest selectivity, compared with digoxin itself, are indicated by double asterisks, and compounds with significant but lower selectivity are shown with a single asterisk. There is a clear peak for the cyclobutyl derivative with four carbon atoms, DcB, with 16.9-, 22.2-, and 33.6-fold selectivity for $\alpha_2\beta_1$, $\alpha_2\beta_2$, and $\alpha_2\beta_3$ over $\alpha_1\beta_1$, respectively. Overall, Table 4 shows that aliphatic substituents with four carbon are most selective (DcB > DMcP >

TABLE 3

Rates of conformational changes for the different isoform complexes determined by stopped-flow measurements

All rates were measured at 23 °C as described under "Experimental Procedures." The turnover rate was calculated from the function $(a \times b)/(a + b)$.

Isoform	$a.$ E$_1$P(3Na) $\rightarrow$ E$_2$P	$b.$ E$_2$(2Rb)ATP $\rightarrow$ E$_1$3 NaATP	Turnover rate	Source
	s^{-1}	s^{-1}	s^{-1}	
$\alpha_1\beta_1$	170.0 $\pm$ 8.0 ($n = 3$)	15.5 $\pm$ 1.2 ($n = 4$)	14.2	Ref. 52
$\alpha_2\beta_1$	91.3 ($n = 2$)	10.2 ($n = 2$)	9.2	Ref. 52
$\alpha_2\beta_2$	58.4 ($n = 2$)	10.3 ($n = 2$)	8.8	This work
$\alpha_2\beta_3$	52.5 ($n = 2$)	10.5 ($n = 2$)	8.8	This work

| R	Derivative	Abbreviation	Theoretical Exact Mass	Mass Found (M + Na$^+$)
-CH$_3$	methyl	DMe	777.47	800.57
-CH$_2$CH$_3$	ethyl	DEt	791.48	814.52
-(CH$_2$)$_2$CH$_3$	propyl	DP	805.50	828.27
-CH(CH$_3$)$_2$	iso-propyl	DiP	805.50	828.41
◁	cyclopropyl	DcP	803.48	826.45
-CH$_2$CH(CH$_3$)$_2$	isobutyl	DiB	819.51	842.66
-CH$_2$-◁	methylcyclopropane	DMcP	817.50	840.44
◇	cyclobutyl	DcB	817.50	840.43
◇NH	azetidinyl	DAz	818.49	841.55
◇S	thietanyl	DTh	835.45	858.37
⬠	cyclopentyl	DcPe	831.51	854.51
⬡	cyclohexyl	DcHe	845.53	868.65
H$_3$C, CH$_3$ ◇	2,2-dimethylcyclobutyl	DcB2,2dM	845.53	868.77
-CH$_2$—◇(CH$_3$)(CH$_3$)	methyl(3,3-dimethylcyclobutane)	DMcB3,3dM	859.54	882.59
-CH$_2$-S(=O)$_2$-CH$_3$	methylsulfonylmethane	DMSM	855.44	878.49
-(CH$_2$)$_2$-S(=O)$_2$-CH$_3$	ethyl-2-sulfonylmethane	DEMS	869.46	892.29
-(CH$_2$)$_2$-S(=O)$_2$-NH$_2$	ethyl-2-sulfonamide	DESA	870.45	893.47

FIGURE 6. **Substituent structures, abbreviated names, and predicted and found masses of perhydro-1,4-oxazepine derivatives of digoxin.**

DiB), whereas the substituents with three carbons (DiP $\approx$ DcP > DP) are also quite selective, and the selectivity ratios decline for substituents with 5, 6, or 7 carbon atoms. The sulfonyl derivatives DMSM, DEMS, and DESA also showed strongly increased selectivity over $\alpha_1\beta_1$ in the order $\alpha_2\beta_3 > \alpha_2\beta_2 > \alpha_2\beta_1$.

Potassium-Cardiac Glycoside Antagonism—CGs bind with high affinity to E$_2$P, and potassium binding causes rapid dephosphorylation to E$_2$(2K), which has a much lower affinity for CGs than E$_2$P (38). Because $K_{0.5}$K$^+$ of $\alpha_2\beta_2$, $\alpha_2\beta_3$ and also $\alpha_2\beta_1$ for activating Na,K-ATPase are higher than for $\alpha_1\beta_1$ in the order $\alpha_2\beta_2 > \alpha_2\beta_3 > \alpha_2\beta_1 > \alpha_1\beta_1$ (Table 1), a higher selectivity for $\alpha_2\beta_2$ and $\alpha_2\beta_3$ and also $\alpha_2\beta_1$ might be due, at least partially, to a weaker K$^+$-CG antagonism. To assess the effect of K$^+$-CG antagonism more systematically, we have measured K_i values for digoxin, the digoxin derivatives and ouabain at increasing K$^+$ concentrations from 2.5, 5, 10, and 20 mM K$^+$. Fig. 7 presents the data for digoxin, but very similar data were obtained for the isobutyl derivative of digoxin (DiB) and also ouabain (not shown). For $\alpha_1\beta_1$, the K_i values increased by 3–4-fold in the range of 2.5–20 mM K$^+$, respectively. By contrast, the K_i values

for $\alpha_2\beta_1$ were much less affected by the increased potassium concentration, and inhibition of $\alpha_2\beta_2$ and $\alpha_2\beta_3$ was essentially unaffected by potassium ions in the range 2.5–20 mM. Consequently, the selectivity for inhibition of $\alpha_2\beta_2$ over $\alpha_1\beta_1$ by digoxin (or other CGs) significantly increased over the range 2.5, 5, 10, and 20 mM potassium from 3.67, 4.77, 11.6, to 15.0, respectively. The differences in K$^+$-digoxin antagonism were also investigated more directly by K$^+$-[^{3}H]digoxin displacement assays (Fig. 8). Yeast membranes harboring either $\alpha_1\beta_1$, $\alpha_2\beta_1$, $\alpha_2\beta_2$, or $\alpha_2\beta_3$ were equilibrated with [^{3}H]digoxin and subsequently incubated with increasing amounts of KCl (up to 150 mM). In the conditions of digoxin binding (with vanadate/magnesium but sodium-free), the apparent $K_{0.5}$K$^+$ for digoxin displacement was 0.62 mM for $\alpha_1\beta_1$ (see also Ref. 25), 1.8 $\pm$ 0.1 mM for $\alpha_2\beta_1$, 2.8 $\pm$ 0.1 mM for $\alpha_2\beta_2$, and 3.2 $\pm$ 0.5 mM for $\alpha_2\beta_3$. Furthermore, at high K$^+$ concentrations, displacement of digoxin binding was incomplete for $\alpha_2\beta_1$, $\alpha_2\beta_2$, and $\alpha_2\beta_3$, the remaining fraction at saturating potassium being 20.3 $\pm$ 1.5, 26 $\pm$ 1.8, and 30.3 $\pm$ 1.5% of control, respectively. Thus, K$^+$-CG antagonism reflects both the affinity for potassium ions and the maximal degree of displacement by potassium ions.

TABLE 4

K_i values and selectivity ratios for the inhibition of purified Na,K-ATPase isoforms by perhydro-1,4-oxazepine derivatives of digoxin

The reaction medium contained 130 mM NaCl, 5 mM KCl, 3 mM MgCl$_2$, 25 mM histidine, pH 7.4, 1 mM EGTA, 0.01 mg/ml SOPS, 0.001 mg/ml cholesterol, and 0.005 mg/ml C$_{12}$E$_8$. Each experiment was carried out at least three times. The calculated K_i values represent averages ± S.E. *, compounds with significantly higher selectivity (K_i $\alpha_1\beta_1/\alpha_2\beta_{1-3}$) than digoxin (>4- and <10-fold). **, compounds with the highest selectivity (K_i $\alpha_1\beta_1/\alpha_2\beta_{1-3}$) compared with digoxin (>12-fold).

	K_i ± S.E.				Selectivity			
CG	$\alpha_1\beta_1$	$\alpha_2\beta_1$	$\alpha_2\beta_2$	$\alpha_2\beta_3$	$\alpha_1\beta_1/\alpha_2\beta_1$	$\alpha_1\beta_1/\alpha_2\beta_2$	$\alpha_1\beta_1/\alpha_2\beta_3$	n
	nM							
Digoxin	268.0 ± 13.8	58.7 ± 5.4	58.0 ± 1.9	42.8 ± 3.0	4.5	4.6	6.2	7
DMe	103.0 ± 5.6	15.3 ± 1.2	20.4 ± 1.8	10.8 ± 0.6	6.7*	5.1	9.5*	7
DEt	137.9 ± 12.6	23.2 ± 0.9	16.4 ± 1.6	14.4 ± 1.3	5.9	8.3*	9.5*	4
DP	87.7 ± 7.9	18.3 ± 1.7	10.5 ± 1.8	9.8 ± 1.1	4.8	8.3*	8.8*	5
DiP	149.0 ± 20.7	28.9 ± 1.7	16.7 ± 1.9	10.3 ± 1.8	5.1	8.9*	14.4**	4
DcP	109.0 ± 6.2	14.6 ± 11.6	13.0 ± 1.3	8.1 ± 1.36	7.5*	8.5*	13.4**	3
DiB	92.0 ± 8.9	20.6 ± 1.4	10.0 ± 0.8	5.8 ± 0.6	4.4	9.0*	16.0**	5
DMcP	95.8 ± 13.7	18.3 ± 1.6	8.0 ± 0.8	4.3 ± 0.6	5.2	12.0**	22.2**	4
DcB	135.0 ± 11.0	8.0 ± 1.3	6.0 ± 1.0	4.0 ± 0.15	16.9**	22.2**	33.6**	3
DAz	222.0 ± 11.6	52.0 ± 1.7	28.0 ± 3.8	26.5 ± 2.3	4.2	7.7*	8.4*	3
DTh	260.0 ± 41.0	108.0 ± 22.6	170.0 ± 10.4	196.0 ± 34.8	2.4	1.5	1.3	3
DcPe	138.0 ± 21.0	33.4 ± 7.5	33.5 ± 11.9	27.6 ± 9.5	4.1	4.1	5.0	3
DcHe	70.4 ± 4.1	15.2 ± 3.7	15.3 ± 2.9	11.7±.5	4.6	4.6	10.1*	3
DcB2,2dM	102.0 ± 4.0	49.0 ± 18.0	39.0 ± 6.0	45.0 ± 14.0	2.1	2.6	2.3	3
DMcB3,3dM	31.6 ± 0.5	8.6 ± 1.4	5.1 ± 0.5	3.9 ± 0.7	3.7	6.2	8.2*	5
DMSM	944.0 ± 123.0	137.0 ± 9.8	123.0 ± 7.3	89.0 ± 8.7	6.9*	7.7*	10.6*	3
DEMS	464.0 ± 14.0	49.2 ± 1.9	31.7 ± 3.2	24.7 ± 2.1	9.4*	14.6**	18.8**	3
DESA	301.0 ± 23.0	38.9 ± 2.2	31.5 ± 4.4	20.1 ± 0.9	7.7*	9.5*	15**	4

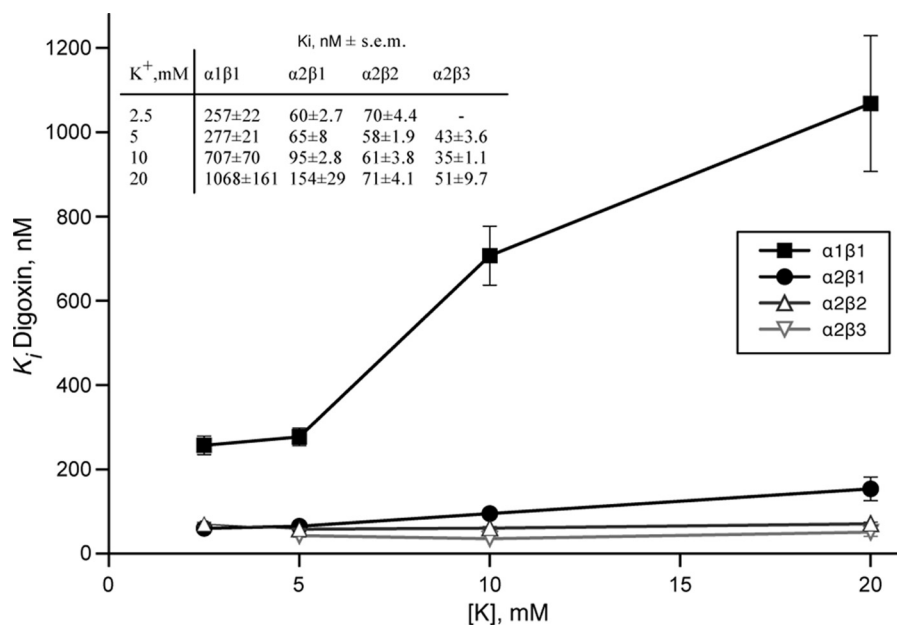| K$^+$,mM	α1β1	α2β1	α2β2	α2β3
			Ki, nM ± s.e.m.	
2.5	257±22	60±2.7	70±4.4	-
5	277±21	65±8	58±1.9	43±3.6
10	707±70	95±2.8	61±3.8	35±1.1
20	1068±161	154±29	71±4.1	51±9.7

FIGURE 7. **Potassium-digoxin antagonism depicted for $\alpha_1\beta_1$, $\alpha_2\beta_1$, $\alpha_2\beta_2$, and $\alpha_2\beta_3$.** Inhibition of purified Na,K-ATPase isoforms by digoxin was measured, and K_i values were plotted against the potassium concentration in the assay medium. *Error bars*, S.E.

Overall, in conditions similar to the extracellular physiological medium (140 mM sodium, 5 mM potassium or with potassium elevated to 20 mM), K-CG antagonism is prominent for $\alpha_1\beta_1$, weak for $\alpha_2\beta_1$ and negligible for $\alpha_2\beta_2$ and $\alpha_2\beta_3$. Note, however, that, in similar conditions, the selectivity ratios for all six derivatives DiB, DMcP, DcB, DMSM, DEMS, and DESA for $\alpha_2\beta_3/\alpha_1\beta_1 > \alpha_2\beta_2/\alpha_1\beta_1 > \alpha_2\beta_1/\alpha_1\beta_1$ are significantly greater than for digoxin itself (Table 4). This shows that reduced K-CG antagonism can indeed account only partially for the increased selectivity for $\alpha_2\beta_3$ and $\alpha_2\beta_2$, whereas the structure of the derivatives is a crucial element determining the isoform selectivity.

Discussion

We discuss here the data showing selective assembly of $\alpha_2\beta_2$ in cardiac myocytes and distinct functional properties and iso-form-selective inhibition of human $\alpha_2\beta_2$ and $\alpha_2\beta_3$, together with possible molecular explanations and physiological or pharmacological implications. Comparisons of functional properties and inhibition of $\alpha_2\beta_1$ with $\alpha_1\beta_1$ reveal the differences between α_2 and α_1, whereas comparisons of $\alpha_2\beta_2$ or $\alpha_2\beta_3$ with $\alpha_2\beta_1$ reveal the influence of β_2 or β_3 compared with β_1. As one general conclusion, it is the combined effects of α_2 and β_2 (or β_3) that give rise to the distinctive functional properties and isoform-selective inhibition of $\alpha_2\beta_2$ (or $\alpha_2\beta_3$).

Specific Assembly of $\alpha_2\beta_2$ in Heart—Three of the four Na,K-ATPase α subunit isoforms and all three β subunit isoforms are expressed in the heart. Although α_1 is the most abundant α subunit isoform, the α_2 isoform rather than the α_1 isoform plays a key role in cardiac muscle contractility by regulating the cytosolic Ca^{2+} concentration in cardiac myocytes. The transient
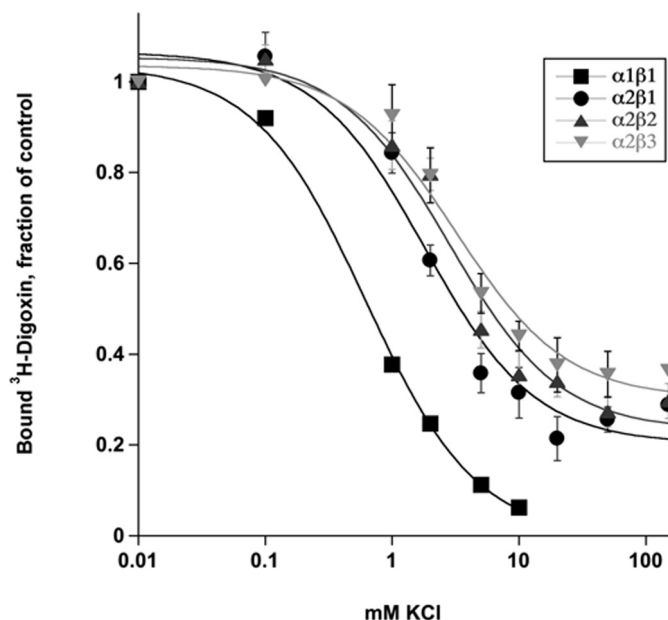
FIGURE 8. **Potassium-[³H]digoxin antagonism.** Yeast membranes harboring $\alpha_2\beta_1$, $\alpha_2\beta_2$, or $\alpha_2\beta_3$ Na,K-ATPase were incubated with varying concentrations of KCl, and residual [³H]digoxin binding was measured. The *lines* represent Hill fits. Data points for $\alpha_1\beta_1$ were taken from Ref. 25. *Error bars*, S.E. from 3 experiments.

rise in Ca^{2+} concentration associated with electrical excitability then triggers cardiac muscle contraction (1). Despite extensive studies of isoform-specific properties of the Na,K-ATPase, the reasons for differential roles of α_2 and α_1 isoforms in cardiac muscle contractility are not fully understood.

The data presented here indicate that the α_2 and β_2 isoforms preferentially assemble with each other in the heart as detected by co-immunoprecipitation (Fig. 3). These data are consistent with previous reports on selective assembly (17) and co-purification of α_2 and β_2 isoforms in the brain (39). Immunofluorescence data in rat and human heart sections indicate that both α_2 and β_2 isoforms specifically localize to the T-tubular membranes, whereas α_1 and β_1 isoforms are distributed in both T-tubular and external sarcolemma membranes (Fig. 1). The data on preferential T-tubular localization of the α_2 and ubiquitous distribution of the α_1 are in agreement with previous reports on measurements of the isoform-specific Na,K-ATPase activity in cardiac myocytes (11, 15, 16, 40) and several immunofluorescence reports (11, 13). On the other hand, our data contrast with several other reports on immunodetection of the Na,K-ATPase α isoforms in the heart (3, 14). The uniform distribution of the β_1 isoform has been reported previously (3), whereas this is the first report describing the specific localization of the β_2 isoform in the heart.

It seems paradoxical that there are two isoform complexes, $\alpha_2\beta_2$ and $\alpha_2\beta_3$, with similar functional properties, as shown in this paper, but in the heart, α_2 assembles with β_2 rather than with β_3. Assembly with a particular β isoform is known to affect trafficking and polarized sorting of the α subunit (19, 41, 42), suggesting that association with the β_2 can be important for the specific location of the α_2 isoform in the T-tubules. Particularly, recombinant addition of *N*-glycosylation sites to the β_1 subunit has been shown to alter localization of the Na,K-ATPase from the basolateral to the apical domain of the plasma membrane in gastric epithelial cells (19). It is possible that eight *N*-glycans *versus* two or three in the β_3 or β_1 isoform play a role in this specific targeting of the α_2 to the microdomains of T-tubular membranes that contain Na^+/Ca^{2+} exchanger and are proximal to other components of Ca^{2+}-regulating complex, which can explain the importance of the α_2 isoform in cardiac muscle contraction.

Another difference between β_3 and β_2 is a role of β_2 in cell adhesion (39, 43). Whether this adhesive role is required for specific location of $\alpha_2\beta_2$ in T-tubules is not clear, but $\alpha_2\beta_2$ differs from $\alpha_2\beta_3$ in this crucial aspect.

Functional Properties of the $\alpha_2\beta_1$, $\alpha_2\beta_2$, and $\alpha_2\beta_3$ Isoform Complexes—The major functional differences between $\alpha_2\beta_2$ and $\alpha_2\beta_3$ when compared with $\alpha_2\beta_1$, and especially $\alpha_1\beta_1$, is the raised $K_{0.5}K^+$ for activating Na,K-ATPase, reduced $K_{0.5}Na^+$, and turnover rate (Table 1). These results confirm previous evidence that α_2 raises $K_{0.5}K^+$ compared with α_1 when it is complexed with β_1 (20, 24, 44) and now show that both β_2 and β_3 lower $K_{0.5}Na^+$ as well as raising $K_{0.5}K^+$ when complexed with α_2, in comparison with complexes with β_1. The RH421 experiments show that the principal mechanism of the effects of α_2 *versus* α_1 and β_2 and β_3 *versus* β_1 to raise $K_{0.5}K^+$ is reduction of the intrinsic binding affinity for potassium ions at the extracellular surface, with $K_{0.5}K^+$ values in the order $\alpha_1\beta_1 < \alpha_2\beta_1 < \alpha_2\beta_3 \leq \alpha_2\beta_2$, respectively (Fig. 5 and Table 2). In RH421 experiments, the potassium affinity is determined in the presence of 50 mM sodium, and, in principle, the reduced affinity for K_{exc} ions could reflect an increased affinity for Na_{exc} and competition with K_{exc}. Nevertheless, displacement of digoxin by potassium ions in the absence of sodium ions ($K_{0.5}K^+$ 0.6 ± 0.07 mM for $\alpha_1\beta_1$, 1.8 ± 0.1 mM for $\alpha_2\beta_1$, 2.8 ± 0.1 mM for $\alpha_2\beta_2$, and 3.2 ± 0.5 mM for $\alpha_2\beta_3$) shows that there is a true and large reduction in intrinsic K_{exc} affinity (Fig. 8). The vanadate titrations with K_i values in the order $\alpha_1\beta_1 < \alpha_2\beta_1 < \alpha_2\beta_3 < \alpha_2\beta_2$ (Table 1) are consistent with the order of decreasing affinities for potassium ions.

Compared with $\alpha_1\beta_1$, $\alpha_2\beta_1$, $\alpha_2\beta_2$, and $\alpha_2\beta_3$ significantly reduced the rate of the conformational transition $E_1P(3Na) \rightarrow E_2P$, with the order $\alpha_1\beta_1 > \alpha_2\beta_1 > \alpha_2\beta_2 \approx \alpha_2\beta_3$ (Fig. 5 and Table 3). In steady-state Na,K-ATPase conditions, a shift of the $E_1P(3Na) \rightarrow E_2P$ conformational equilibrium toward E_1P would contribute to the higher $K_{0.5}K^+$ as well as lower $K_{0.5}Na^+$ (and higher K_i vanadate) (Table 1). Note that the reduced $K_{0.5}Na^+$ of $\alpha_2\beta_2$ and $\alpha_2\beta_3$ compared with $\alpha_1\beta_1$ and $\alpha_2\beta_1$ is not explained by a change in intrinsic binding affinity for sodium ions (see Fig. 5A).

$\alpha_2\beta_1$ also displayed a reduced rate of $E_2(2Rb)ATP \rightarrow E_1(3Na)ATP$ when compared with $\alpha_1\beta_1$, but there was no further decrease in $\alpha_2\beta_2$ and $\alpha_2\beta_3$. This finding explains the reduced turnover rate for all α_2 complexes compared with α_1. The different β isoforms appear to have no isoform-selective influence on the turnover rate, which is governed by the slow rate-determining step $E_2(2Rb)ATP \rightarrow E_1(3Na)ATP$, reduced by α_2, and not by the faster $E_1P(3Na) \rightarrow E_2P$ transition.

In the absence of high resolution structures of the α_2 complexes, one can only speculate on possible explanations of the kinetic effects of α_2 and β_2 or β_3, such as the reduced K_{exc}
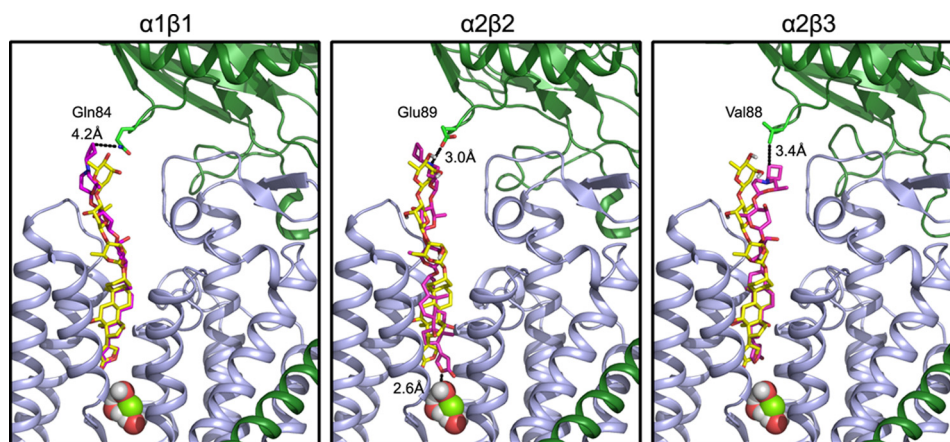
FIGURE 9. **Models for docking of DcB to $\alpha_1\beta_1$, $\alpha_2\beta_2$, and $\alpha_2\beta_3$.** DcB was docked into homology models of human Na,K-ATPase isoforms derived from the porcine E2P·Mg·digoxin structure (Protein Data Bank code 4RET) as described under "Experimental Procedures." α and β subunits are shown in *green* and *blue ribbon representations*. Transmembrane helices 3 and 5 of the α-subunit are removed for clarity. Digoxin (*yellow*) and DcB (*purple*) are shown in a *stick representation*, and water and a magnesium ion are shown as *spheres*. The residues of the β subunit closest to the cyclobutyl moiety, β_1Gln-84, β_2Glu-89, and β_3Val-88, are shown as *sticks*, and distances to DcB are indicated.

binding affinity. Using chimeras of Na,K-ATPase and H,K-ATPase, the extracellular domain was identified as the main modifier of the apparent potassium affinity (for displacing bound ouabain) (45), and the main interaction site was shown to be an SYGQ motif in the M7-8 loop of α (46). In an older study (47), the extracellular domain of β_1 was suggested to cover the extracellular domain of the α subunit and control access to the Rb(K) binding sites. In general, this concept appears compatible with the molecular structures of Na,K-ATPase ($\alpha_1\beta_1$) (48–50). Thus, compared with $\alpha_1\beta_1$, the K_{exc} entry and exit pathway may be more accessible in $\alpha_2\beta_1$ itself and even more so in $\alpha_2\beta_2$ and $\alpha_2\beta_3$, leading to the large decrease in K_{exc} binding affinity.

Digoxin Derivatives with Strong Selectivity for $\alpha_2\beta_2$ and $\alpha_2\beta_3$ Complexes—The conclusion from all of the experiments in Table 4 is that digoxin perhydro-1,4-oxazepine derivatives with four carbon substitutions (cyclobutyl (DcB), methyl cyclopropyl (DMcP), and isobutyl (DiB)) have the highest selectivity for $\alpha_2\beta_3/\alpha_1\beta_1$ and $\alpha_2\beta_2/\alpha_1\beta_1$ compared with compounds with 1–3 or 5 or a greater number of carbon atom substitutions. This confirms the data in Ref. 26 for $\alpha_2\beta_3/\alpha_1\beta_1$ and extends them to $\alpha_2\beta_2/\alpha_1\beta$. The optimal size of the aliphatic substituents (four carbon atoms), cyclic and non-cyclic, may indicate a size restriction of the space between the α and β subunits. Replacement of one methylene group in the cyclobutyl DcB with a single NH (DAz) or sulfur (DTh) atom strongly reduces selectivity, whereas the three new sulfonyl derivatives, DMSM, DEMS, and DESA, showed enhanced selectivity for $\alpha_2\beta_2$ and $\alpha_2\beta_3$ and to some extent also $\alpha_2\beta_1$, relative to digoxin itself (Table 4). Thus, the highest selectivity for the $\alpha_2\beta_2$ and $\alpha_2\beta_3$ isoform complexes depends crucially on the structure of the derivatives, providing the strongest evidence for selective interactions of the substituent groups with β_2 and β_3, respectively.

We have attempted to explain the selectivity of DcB for $\alpha_2\beta_3$ and $\alpha_2\beta_2$ with molecular docking models, starting with a structure of renal Na,K-ATPase ($\alpha_1\beta_1$) with bound digoxin (51) (Protein Data Bank code 4RET) (Fig. 9). The models display the optimal positions found for DcB relative to digoxin and emphasize the major attractive interactions, particularly with the β

subunit. The modeling supports the experimental result whereby DcB binds to $\alpha_2\beta_3$ with the highest potency and selectivity, showing a hydrophobic interaction between the DcB-cyclobutyl moiety and β_3Val-88. There is also an electrostatic interaction of the protonated nitrogen of perhydro-1,4-oxazepine ring with Asp-889 of α_2. In the case of $\alpha_2\beta_2$, to which DcB also binds with good potency and selectivity, the modeling shows a hydrogen bond interaction between the protonated perhydro-1,4-oxazepine ring nitrogen and β_2Glu-89 and also an additional hydrogen bond between the lactone ring and the structural water molecule located at the bottom of the binding site. It is noticeable that the steroid and lactone moieties are somewhat rotated compared with the digoxin itself. By contrast with the $\alpha_2\beta_3$ and $\alpha_2\beta_2$ models, in the $\alpha_1\beta_1$ model, the steroid-lactone moiety of DcB almost exactly overlaps that of digoxin and displays only a weak interaction with β_1Gln-84. This result also appears to be consistent with the experimental result for $\alpha_1\beta_1$ which displays a much lower potency for DcB and only a small difference from digoxin itself.

Taken together, it is evident that both the α and the β subunits determine the selectivity of the digoxin derivatives, and the β subunit, in particular, has favorable interactions with the substituted third sugar residue.

Physiological Role of $\alpha_2\beta_2$—In relation to the physiological function, major differences of $\alpha_2\beta_2$ compared with $\alpha_1\beta_1$ include the high $K_{0.5}K^+$ values (low affinity) for extracellular potassium ions, a somewhat lower turnover rate, and a significantly lower $K_{0.5}Na^+$. Although the current experiments have been done with detergent-soluble purified proteins, a very similar effect of $\alpha_2\beta_2$ to strongly raise $K_{0.5}K^+$ values for extracellular potassium ions compared with $\alpha_1\beta_1$ and also $\alpha_2\beta_1$ has been described with the proteins expressed in *Xenopus* oocytes (20, 21, 52). A property that we cannot assess in experiments with detergent-soluble proteins is the dependence of activity on membrane potential. As described previously (20), $\alpha_2\beta_1$ shows a steeper dependence on voltage than $\alpha_1\beta_1$ or $\alpha_3\beta_1$, and recent work shows that $\alpha_2\beta_2$ shows a particularly steep dependence (21). The voltage dependence of the pump current in physiological conditions is mainly a reflection of Na^+_{exc}-mediated

competition with K^+_{exc} leading to inhibition at negative potentials. The conditions of our experiments are equivalent to those in cells at 0 mV membrane potential, and compared with physiological conditions, the raised $K_{0.5}K^+$ of $\alpha_2\beta_2$ represents, if anything, an underestimated value compared with $\alpha_1\beta_1$. At physiological K^+_{exc} of 4.5 mM and resting membrane potentials in the heart or skeletal muscle or brain glial cells (-70 to 90 mV), $\alpha_2\beta_2$ is largely inactive. Thus, $\alpha_2\beta_2$ acts as a "reserve pump," which responds to acutely increased K^+_{exc} or positive membrane potentials by increasing its rate and moderating the changes in K^+_{exc} and then restoring the ion gradients after the change (see Refs. 52 and 53). For example, increased activity of skeletal muscles leads to loss of potassium ions and a large increase in K^+_{exc}, which can reach as high as 8.3 mM in serum, 10–12 mM in muscle interstitial fluid, and locally as high as 25 mM in T-tubules (54). In heart muscle, the $\alpha_2\beta_2$ is also almost inactive at resting potentials but becomes acutely activated during raised cardiac activity due to the fact that the membrane potential is positive for a significant fraction of the time during the extended action potentials (21). As in skeletal muscle, the potassium concentration in T-tubules can be presumed to rise significantly. The lower $K_{0.5}Na^+$ of $\alpha_2\beta_2$ should also contribute significantly to rapid restoration of the sodium gradient associated with increased activity and raised cytoplasmic sodium. Due to coupling of the sodium fluxes mediated by $\alpha_2\beta_2$ with sodium and calcium fluxes mediated by NCX1, the kinetic features of $\alpha_2\beta_2$ described are expected to play an important role in regulation of the calcium dynamics of active *versus* resting cardiac muscle. Indeed, an important role of α_2 overexpression in calcium dynamics in myocytes, associated with a decreased $K_{0.5}Na^+$, has been proposed recently (55), although it was not known which β isoform is coupled with α_2. The $\alpha_1\beta_1$ complex maintains ion gradients in resting conditions but is not suited for the regulatory role of $\alpha_2\beta_2$ just discussed because the potassium sites ($K_{0.5}K^+ = 1.5 \pm 0.1$ mM) are almost saturated even in resting conditions, and the voltage dependence of $\alpha_1\beta_1$ is shallow.

Pharmacological Implications—As discussed in the Introduction, an α_2-selective CG could be an efficient inotropic agent. The present findings have the additional interesting implication that an $\alpha_2\beta_2$-selective CG, such as the digoxin derivatives described here, could also have reduced cardiotoxicity compared with digoxin.

For many years, digoxin was used routinely to treat heart failure, due to its inotropic and chronotropic effects, but it is now used much less on account of the narrow therapeutic range and cardiotoxicity resulting from the well known phenomena of calcium overload and cardiac arrhythmias (31). The incidence of digitalis toxicity has decreased in parallel with its decreased use (56). The main cause of digitalis toxicity is accumulation of digoxin, secondary to decreased renal function, and a major exacerbating factor is hypokalemia, which is prevalent in subjects treated with diuretics in addition to digitalis (56) (for a recent study, see Ref. 57). Indeed, due to the potentiation of digitalis toxicity by hypokalemia, it was even recommended, in the past, to treat severe cases by raising serum potassium (58). The salient present finding is that inhibition of $\alpha_1\beta_1$ by digoxin and all other CGs is strongly antagonized by raising

potassium in the range of 2.5–20 mM, whereas $\alpha_2\beta_2$ is unaffected (Fig. 7). Assuming that digoxin toxicity *in vivo*, exacerbated by hypokalemia, is associated with excessive Na,K-pump inhibition, this implies that toxicity is indeed mediated by $\alpha_1\beta_1$. Conversely, the insensitivity of inhibition of $\alpha_2\beta_2$ to potassium (2.5–20 mM) would imply that $\alpha_2\beta_2$ does not play a major role in digitalis toxicity. This conclusion fits well with the rationale that $\alpha_2\beta_2$-selective derivatives could be effective positive inotropic agents and also have reduced toxic effects.

Considerable evidence exists for the presence of endogenous CG-like compounds in mammalian tissues, such as ouabain or marinobufagenin, that may serve to regulate Na,K-ATPase activity (59–61). Our unpublished experiments show a higher sensitivity of $\alpha_2\beta_2$ over $\alpha_1\beta_1$ for ouabain ($K_i = 63.7 \pm 9.8$ *versus* 153.0 ± 11.6 nM, respectively),[7] suggesting that endogenous ouabain-like compounds may bind more efficiently to $\alpha_2\beta_2$ isoform and thus specifically regulate the $\alpha_2\beta_2$ ion pumping activity or α_2-dependent signaling pathways. In particular, α_2-mediated signaling may explain a specific role of the α_2 subunit in the modulation of blood pressure under stress conditions (60–63).

Conclusions—In summary, our data demonstrate the specific association of the Na,K-ATPase α_2 isoform with the β_2 and the specific intracellular location of the $\alpha_2\beta_2$ heterodimer. The distinct functional properties of human $\alpha_2\beta_2$ are consistent with an important regulatory role in cardiac muscle contraction. Furthermore, isoform-selective inhibition by digoxin derivatives, such as DcB, suggests that they could be safer cardiac inotropic agents compared with digoxin itself.

Experimental Procedures

Materials

n-Dodecyl-β-D-maltopyranoside (catalogue no. D310) and $C_{12}E_8$ (25% (w/w), catalogue no. 0330) were purchased from Anatrace, and BD-Talon metal affinity resin was from Clontech (catalogue no. 635503). 1-Stearoyl-2-oleoyl-*sn*-glycero-3-phospho-L-serine (SOPS) was purchased from Avanti Polar Lipids. PiColorLock™ was purchased from Innova Bioscience, and RH421 was from MoBiTec. All other reagents were purchased from Merck or Sigma-Aldrich at the highest quality level available.

Primary Antibodies—For immunofluorescent staining, the following monoclonal antibodies were used: Na,K-ATPase α_1 subunit (mouse, clone C464.6, 1:20; Millipore) and Na,K-ATPase β_1 subunit (mouse, clone M17 P5 F11, 1:100; Affinity Bioreagents). The polyclonal antibodies used were Na,K-ATPase α_2 subunit (rabbit, 1:200; Millipore) and Na,K-ATPase β_2 subunit (rabbit, 1:200; Millipore).

For Western blotting analysis, the following monoclonal antibodies were used: against the Na,K-ATPase α_1 subunit (mouse, clone C464.6, 1:1000; Millipore), against the Na,K-ATPase β_2 subunit (mouse, clone 35; BD Transduction Laboratories), and Na,K-ATPase β_3 subunit (goat, 1:500; Santa Cruz Biotechnology, Inc.). Na,K-ATPase β_1 subunit polyclonal antibody (rabbit; 1:5000) was a generous gift of Dr. W. James Ball, Jr. (University of Cincinnati).

---

[7] A. Katz, O. Vagin, and S. J. D. Karlish, unpublished results.

Assembly, Function, and Selective Inhibition of Na,K-ATPase $\alpha_2\beta_2$

Methods

Confocal Microscopy—Confocal microscopy images were acquired using the Zeiss LSM 510 laser scanning confocal microscope and ZEN 2009 software.

Isolation of Membrane Fractions from Mouse Heart—Mouse heart was homogenized with a tight Dounce homogenizer (Wheaton, Millville, NY). Cell debris was removed by centrifugation ($2000 \times g$, 10 min). The cleared homogenate was layered onto a 42% sucrose solution in 10 mM PIPES, 2 mM EGTA, 2 mM EDTA, pH 7.0, and spun in a Beckman SW28 swinging bucket rotor at 25,000 rpm for 1 h at 4 °C. The fraction at the interface of buffer/sucrose was collected and diluted to a total volume of 15 ml of 10 mM PIPES, 2 mM EGTA, 2 mM EDTA, pH 7.0. Membranes were spun down by centrifugation in a Beckman 75Ti rotor (35,000 rpm, 4 °C, 1 h). The pellet was resuspended in 10 mM PIPES/Tris buffer containing 2 mM EGTA and 2 mM EDTA, pH 7.0, by homogenization with a 2-ml Teflon homogenizer (Wheaton). The membranes were aliquoted, flash-frozen, and stored at −80 °C. Proteins were extracted by incubating membranes with 50 mM Tris, pH 7.5, containing 150 mM NaCl, 1% Nonidet P-40, 0.5% sodium deoxycholate, and complete protease inhibitor mixture (1 tablet/50 ml at 4 °C for 30 min). Membrane extracts were clarified by centrifugation ($100,000 \times g$, 1 h) at 4 °C. Where indicated, protein extracts were treated by PNGase F from *Flavobacterium meningosepticum* (New England Biolabs) according to the manufacturer's instructions before loading on SDS-PAGE.

Immunoprecipitation—Protein extracts from mouse heart membrane fractions (100–300 μg of protein) were incubated with 30 μl of the protein A-agarose suspension (Roche Diagnostics) in a total volume 1 ml of the extraction buffer at 4 °C with continuous rotation for at least 3 h (or overnight) to remove the components that non-specifically bind to protein A. The precleared cell extract was mixed with 10 μl of polyclonal antibodies against the Na,K-ATPase α_2 subunit (Millipore) or 10 μl of polyclonal antibodies against the Na,K-ATPase α subunit (64) or 10 μl of polyclonal antibodies against the Na,K-ATPase β_2 subunit (Millipore) and incubated with continuous rotation at 4 °C for 60 min. After the addition of 30 μl of the protein A-agarose suspension, the mixture was incubated at 4 °C with continuous rotation overnight. The bead-adherent complexes were washed three times on the beads and then eluted as described previously (65).

Where indicated, the bead-adherent proteins were treated with PNGase F. Deglycosylation by PNGase F was performed by incubation of the bead-adherent proteins with 1 μl of PNGase F in 30 μl of 50 mM sodium phosphate, pH 7.5, containing 1% Nonidet P-40 at 37 °C for 1 h. After incubation with glycosidases, the reaction mixture was separated from the beads. The adherent proteins were eluted from the beads by incubation in 30 μl of 2× SDS-PAGE sample buffer for 5 min at 80 °C. To account for possible dissociation of immunoprecipitated proteins from the beads during deglycosylation, the eluted proteins were combined with the reaction mixture. After separation by SDS-PAGE, the immunoprecipitated and co-immunoprecipitated proteins were analyzed by Western blotting by using appropriate antibodies.

Western Blotting Analysis—1–10 μg of proteins extracted from mouse heart membranes or 5–20 μl of proteins eluted from the protein A-conjugated agarose beads were loaded onto 4–12% gradient SDS-polyacrylamide gels (Invitrogen). Proteins were separated by SDS-PAGE, transferred onto a nitrocellulose membrane (Bio-Rad), and detected by Western blotting analysis as described previously (65).

Immunofluorescent Staining—Mouse embryo sections and frozen tissue sections on FDA standard frozen tissue rat or human arrays (BioChain) were incubated with Dako Protein Block serum-free solution (Dako Corp.) for 30 min. Immunofluorescent staining was performed by a 1-h incubation with the primary antibodies followed by a 1-h incubation with Alexa Fluor 633- or Alexa Fluor 488-conjugated anti-mouse or anti-rabbit antibodies (Invitrogen).

Plasmid Construction for the Expression of $\alpha_2\beta_2$ $\alpha_2\beta_3$ Na,K-ATPase—Generation of pHil-D2 expression vector containing cDNA of human α_1 and His$_{10}$-tagged porcine (p) or human (h) β_1 was described previously (35). cDNAs of human β_2 and β_3 in pSD5 were a gift from K. Geering (University Lausanne, Switzerland). Open reading frames and flanking regions of human β_2 and β_3 were amplified by PCR using primers containing BglII and SalI cleavage sites. The resulting fragments were subcloned into pHil-D2-hα_2/His$_{10}$-pβ_1 to create pHil-D2-hα_2/His$_{10}$-hβ_2 and pHil-D2-hα_2/His$_{10}$-hβ_3, respectively. Correct integration and sequence was confirmed by sequencing.

Yeast transformation and clone selection have been described in detail (35). *P. pastoris* SMD1165 was grown in BMG (100 mM potassium phosphate, pH 6, 1.34% yeast nitrogen base, 4×10^{-5}% biotin, 0.3% glycerol) to OD 6–8, and expression was induced in BMM (100 mM potassium phosphate, pH 6, 1.34% yeast nitrogen base, 4×10^{-5}% biotin, 0.5% methanol added daily). Yeasts were transformed with linearized pHil-D2-human α_2-human His$_{10}$-β_2 or human His$_{10}$-β_3, and His$^+$/Mut^S clones were selected and grown at 20 °C for 3 days in baffled Erlenmeyer flasks, as described previously for $\alpha_1\beta_1$ and $\alpha_2\beta_1$ (35, 66). Under these conditions, only weak expression was observed for $\alpha_2\beta_2$ and $\alpha_2\beta_3$. It was then determined that expression of both $\alpha_2\beta_3$ and $\alpha_2\beta_2$ was transient and peaked between 15 and 19 h for $\alpha_2\beta_3$ and between 16 and 28 h for $\alpha_2\beta_2$. Further screening of expression temperature revealed 23 °C to be optimal. This transient expression was not observed for $\alpha_1\beta_1$, $\alpha_2\beta_1$, and $\alpha_3\beta_1$ that were stably expressed for 3–5 days, which also resulted in a higher cell density and protein yield per liter of culture. To overcome this limitation for $\alpha_2\beta_3$ and $\alpha_2\beta_2$, the following three-phase growth/induction protocol was used. In phase I, glycerol batch cultivation, yeasts were grown in BMG in an aerated 10-liter vessel until OD reached 6–8. In phase II, the glycerol-fed batch phase, 0.05% glycerol/h was added to the culture. Glycerol feeding was continued until OD reached 13–15. Extending the fed batch to higher cell densities often led to excessive foaming and a loss of cells. In phase III, the induction phase, expression was induced by adding 0.5% methanol/day. No increase of OD was observed during this phase. All three phases were carried out at 23 °C. In addition to the increase in cell density, fed batch cultivation increased expression levels of Na,K-ATPase. Membranes prepared from

cells grown in baffled spinner flasks showed >30% higher specific ouabain binding when compared with membranes from cells that did not undergo fed batch cultivation. The same increase was observed in Western blots of these membranes, indicating that most of the expressed protein was properly folded and functional.

Expression and Purification of $\alpha_1\beta_1$FXYD1, $\alpha_2\beta_1$FXYD1, $\alpha_2\beta_2$FXYD1, and $\alpha_2\beta_3$FXYD1 Complexes—The experiments have utilized the purified detergent-soluble $\alpha\beta$FXYD1 complexes rather than the $\alpha\beta$ complexes alone, because FXYD1 strongly stabilizes the proteins against thermal inactivation (67) and does not affect inhibition by ouabain or digoxin (25, 68). Membrane preparation and His tag purification on BD-Talon beads of recombinant human $\alpha_1\beta_1$FXYD1 and $\alpha_2\beta_1$FXYD1 Na,K-ATPase were done essentially as described previously (69–71). Yeast membrane expression and purification of recombinant $\alpha_2\beta_2$ and $\alpha_2\beta_3$ Na,K-ATPase were similar except where indicated (for details, see "Results"). Human FXYD1 was expressed in *Escherichia coli* and purified and reconstituted with $\alpha\beta$ complexes on the beads to yield $\alpha\beta$FXYD1 complexes (35, 67, 71). Elution buffers consisted of 200 mM imidazole, 100 mM NaCl, 20 mM MOPS/Tris, pH 7.4, 0.1 mg/ml $C_{12}E_8$, 0.01 mg/ml cholesterol, and 0.07 mg/ml SOPS. 25% glycerol was added, and the soluble protein complexes were stored at -80 °C.

Biochemical Assays—ATPase activity assays as well as titrations with NaCl, KCl, and vanadate were performed as described previously (29, 35) using PiColorLock^{TM} malachite green assay (Innova Bioscience). For ion titrations, activity was measured at varying concentrations of sodium plus choline chloride and KCl (80 mM), with constant total ionic strength (170 mM total). $K_{0.5}Na^+$ and $K_{0.5}K^+$ values were obtained by fitting the data to the Hill equation using KaleidaGraph (Synergy Software) (30).

Inhibition of Na,K-ATPase activity and [^{3}H]ouabain binding and K-[^{3}H]digoxin displacement assays were performed as reported (25). For derivation of K_i values, percentage inhibition of Na,K-ATPase activity, VCG/V0, was calculated, and K_i values were obtained by fitting the data to the function, VCG/V0 = $K_i/([CG] + K_i) + c$. Inhibition was estimated in 3–7 separate experiments, and average K_i values ± S.E. were calculated (27).

Equilibrium and Stopped-flow Fluorescence Measurements Using RH421—Equilibrium fluorescence experiments were carried out in a Varian fluorimeter at room temperature. 10 μg of purified Na,K-ATPase was added to 1 ml of 20 mM MOPS/Tris, pH 7.2, 5 mM MgCl$_2$, and 200 nM RH421. NaCl, ATP, and KCl where then added successively. NaCl and KCl titrations were performed as described previously (37) with emission and excitation wavelength set to 580 and 680 nm with a 5-nm slit width.

Stopped-flow measurements were made using an Applied Photophysics SX20 system (see Ref. 29). Using a combined xenon/mercury lamp, excitation wavelength was 577 nm, and fluorescence was measured at $\geq$665 nm using cut-off filters. Solutions were mixed 1:1 using ~120 μl/syringe, and the temperature of the measurements was set to 23 °C. All solutions were buffered to pH 7.2 using MOPS/Tris, and ionic strength

was kept constant at 120 mM for all measurements using choline chloride.

For measurement of E2(2Rb)ATP → E1·3NaATP, syringe 1 contained 20 μg/ml enzyme non-covalently labeled with 200 nM RH421 in 20 mM RbCl, 1 mM EDTA and was mixed with 80 mM NaCl, 2 mM ATP, 1 mM EDTA in syringe 2. For measurement of E1·3Na → E2P, 10 μg/ml Na,K-ATPase non-covalently labeled with 200 nM RH421 in 100 mM NaCl and 4 mM MgCl$_2$ in syringe 1 was mixed with 1 mM ATP in the same solution in syringe 2.

Data were fitted using KaleidaGraph (Synergy Software). Ion titrations were fitted using the Hill equation,

$$\Delta F = \frac{\Delta F_{max}}{1 + \left(\frac{K_{1/2}}{[\text{ion}]}\right)^n}$$ (Eq. 1)

where n is the Hill coefficient, [ion] is the free concentration of the respective ion, and $K_{1/2}$ is the concentration required to obtain the half-maximal fluorescence signal.

Stopped-flow traces were fitted to a monoexponential function,

$$F = A \cdot e^{-k \cdot t} + c$$ (Eq. 2)

or double exponential function,

$$F = A_1 \cdot e^{-k_1 \cdot t} + A_2 \cdot e^{-k_2 \cdot t} + c$$ (Eq. 3)

where A is the amplitude of the fluorescence signal, k is the rate of the reaction, and c is the equilibrium fluorescence level after the reaction is complete. All values are expressed as averages of 2–4 experiments.

Molecular Modeling—Homology modeling of human Na,K-ATPase $\alpha_2\beta_1$, $\alpha_2\beta_2$, and $\alpha_2\beta_3$ isoform complexes was carried out using the template $\alpha_1\beta_1$ with bound digoxin (Protein Data Bank code 4RET) as described previously (26). The final model exhibits the highest Profiles 3D score (72) and the lowest number of Ramachandran violations (73). Rather consistent profiles were observed for each model ($\alpha_2\beta_1$, $\alpha_2\beta_2$, and $\alpha_2\beta_3$), demonstrating that the human Na,K-ATPase models were reasonable and could be employed for the further docking study. The magnesium ion and three structural waters were positioned in each final model. Models were eventually refined by energy minimization using the CHARMm force field (74).

Molecular Docking—Molecular docking of DcB to the different human Na,K-ATPase isoform models was carried out in Discovery Studio version 4.0 (Biovia, Dassault Systemes, San Diego, CA) with CDOCKER, which is an implementation of a CHARMm-based docking tool using a rigid receptor (75). The DcB ligand was prepared before docking using the Prepare Ligand module to evaluate ionization states for a given pH, isomers, and tautomers, correct bad valences, and generate three-dimensional conformations. The digoxin bioactive binding conformation was copied from the 4RET crystal structure and positioned into each model. The model binding site was defined as a sphere with radius that stays within 15 Å from the geometric centroid of the digoxin ligand using the Define and Edit Binding Site tool.

DcB was docked into the active site of each Na,K-ATPase human model. Different ligand orientations were generated, and for each orientation, the CHARMm energy (interaction energy plus ligand strain) and the interaction energy alone were calculated. The ligand orientations were sorted by CHARMM energy, and the top scoring (most negative, thus favorable to binding) orientations were retained. The final orientations selected were chosen based on their docking scores, which favor interactions with amino acids from the β subunit.

Synthesis of Digoxin Derivatives—Detailed protocols for synthesis, purification, and analysis of perhydro-1–4-oxazepine derivatives of digoxin have been described previously (26, 27, 76).

References

1. Bers, D. M. (2008) Calcium cycling and signaling in cardiac myocytes. *Annu. Rev. Physiol.* **70**, 23–49
2. Harada, K., Lin, H., Endo, Y., Fujishiro, N., Sakamoto, Y., and Inoue, M. (2006) Subunit composition and role of Na$^+$,K$^+$-ATPases in ventricular myocytes. *J. Physiol. Sci.* **56**, 113–121
3. McDonough, A. A., Zhang, Y., Shin, V., and Frank, J. S. (1996) Subcellular distribution of sodium pump isoform subunits in mammalian cardiac myocytes. *Am. J. Physiol.* **270**, C1221–C1227
4. Sweadner, K. J., Herrera, V. L., Amato, S., Moellmann, A., Gibbons, D. K., and Repke, K. R. (1994) Immunologic identification of Na$^+$,K$^+$-ATPase isoforms in myocardium: isoform change in deoxycorticosterone acetate-salt hypertension. *Circ. Res.* **74**, 669–678
5. Geering, K. (2006) FXYD proteins: new regulators of Na-K-ATPase. *Am. J. Physiol. Renal Physiol.* **290**, F241–F250
6. Pavlovic, D., Fuller, W., and Shattock, M. J. (2013) Novel regulation of cardiac Na pump via phospholemman. *J. Mol. Cell. Cardiol.* **61**, 83–93
7. Despa, S., Lingrel, J. B., and Bers, D. M. (2012) Na$^+$/K$^+$-ATPase α_2-isoform preferentially modulates Ca^{2+} transients and sarcoplasmic reticulum Ca^{2+} release in cardiac myocytes. *Cardiovasc. Res.* **95**, 480–486
8. Dostanic, I., Paul, R. J., Lorenz, J. N., Theriault, S., Van Huysse, J. W., and Lingrel, J. B. (2005) The α_2-isoform of Na-K-ATPase mediates ouabain-induced hypertension in mice and increased vascular contractility *in vitro*. *Am. J. Physiol. Heart Circ. Physiol.* **288**, H477–H485
9. James, P. F., Grupp, I. L., Grupp, G., Woo, A. L., Askew, G. R., Croyle, M. L., Walsh, R. A., and Lingrel, J. B. (1999) Identification of a specific role for the Na,K-ATPase α_2 isoform as a regulator of calcium in the heart. *Mol. Cell* **3**, 555–563
10. Shattock, M. J., Ottolia, M., Bers, D. M., Blaustein, M. P., Boguslavskyi, A., Bossuyt, J., Bridge, J. H., Chen-Izu, Y., Clancy, C. E., Edwards, A., Goldhaber, J., Kaplan, J., Lingrel, J. B., Pavlovic, D., Philipson, K., Sipido, K. R., and Xie, Z. J. (2015) Na$^+$/Ca^{2+} exchange and Na$^+$/K$^+$-ATPase in the heart. *J. Physiol.* **593**, 1361–1382
11. Swift, F., Tovsrud, N., Enger, U. H., Sjaastad, I., and Sejersted, O. M. (2007) The Na$^+$/K$^+$-ATPase α_2-isoform regulates cardiac contractility in rat cardiomyocytes. *Cardiovasc. Res.* **75**, 109–117
12. Juhaszova, M., and Blaustein, M. P. (1997) Distinct distribution of different Na$^+$ pump α subunit isoforms in plasmalemma: physiological implications. *Ann. N.Y. Acad. Sci.* **834**, 524–536
13. Silverman, B. Z., Fuller, W., Eaton, P., Deng, J., Moorman, J. R., Cheung, J. Y., James, A. F., and Shattock, M. J. (2005) Serine 68 phosphorylation of phospholemman: acute isoform-specific activation of cardiac Na/K ATPase. *Cardiovasc. Res.* **65**, 93–103
14. Mohler, P. J., Davis, J. Q., and Bennett, V. (2005) Ankyrin-B coordinates the Na/K ATPase, Na/Ca exchanger, and InsP3 receptor in a cardiac T-tubule/SR microdomain. *PLoS Biol.* **3**, e423
15. Berry, R. G., Despa, S., Fuller, W., Bers, D. M., and Shattock, M. J. (2007) Differential distribution and regulation of mouse cardiac Na$^+$/K$^+$-ATPase α_1 and α_2 subunits in T-tubule and surface sarcolemmal membranes. *Cardiovasc. Res.* **73**, 92–100
16. Despa, S., and Bers, D. M. (2007) Functional analysis of Na$^+$/K$^+$-ATPase isoform distribution in rat ventricular myocytes. *Am. J. Physiol. Cell Physiol.* **293**, C321–C327
17. Tokhtaeva, E., Clifford, R. J., Kaplan, J. H., Sachs, G., and Vagin, O. (2012) Subunit isoform selectivity in assembly of Na,K-ATPase α-β heterodimers. *J. Biol. Chem.* **287**, 26115–26125
18. Tokhtaeva, E., Sachs, G., and Vagin, O. (2009) Assembly with the Na,K-ATPase α_1 subunit is required for export of β_1 and β_2 subunits from the endoplasmic reticulum. *Biochemistry* **48**, 11421–11431
19. Vagin, O., Turdikulova, S., and Sachs, G. (2005) Recombinant addition of N-glycosylation sites to the basolateral Na,K-ATPase beta1 subunit results in its clustering in caveolae and apical sorting in HGT-1 cells. *J. Biol. Chem.* **280**, 43159–43167
20. Crambert, G., Hasler, U., Beggah, A. T., Yu, C., Modyanov, N. N., Horisberger, J. D., Lelièvre, L., and Geering, K. (2000) Transport and pharmacological properties of nine different human Na,K-ATPase isozymes. *J. Biol. Chem.* **275**, 1976–1986
21. Stanley, C. M., Gagnon, D. G., Bernal, A., Meyer, D. J., Rosenthal, J. J., and Artigas, P. (2015) Importance of the voltage dependence of cardiac Na/K ATPase isozymes. *Biophys. J.* **109**, 1852–1862
22. Figtree, G. A., Liu, C. C., Bibert, S., Hamilton, E. J., Garcia, A., White, C. N., Chia, K. K., Cornelius, F., Geering, K., and Rasmussen, H. H. (2009) Reversible oxidative modification: a key mechanism of Na$^+$-K$^+$ pump regulation. *Circ. Res.* **105**, 185–193
23. Howie, J., Tulloch, L. B., Shattock, M. J., and Fuller, W. (2013) Regulation of the cardiac Na$^+$ pump by palmitoylation of its catalytic and regulatory subunits. *Biochem. Soc. Trans.* **41**, 95–100
24. Blanco, G., Koster, J. C., Sánchez, G., and Mercer, R. W. (1995) Kinetic properties of the $\alpha_2\beta_1$ and $\alpha_2\beta_2$ isozymes of the Na,K-ATPase. *Biochemistry* **34**, 319–325
25. Katz, A., Lifshitz, Y., Bab-Dinitz, E., Kapri-Pardes, E., Goldshleger, R., Tal, D. M., and Karlish, S. J. (2010) Selectivity of digitalis glycosides for isoforms of human Na,K-ATPase. *J. Biol. Chem.* **285**, 19582–19592
26. Katz, A., Tal, D. M., Heller, D., Habeck, M., Ben Zeev, E., Rabah, B., Bar Kana, Y., Marcovich, A. L., and Karlish, S. J. (2015) Digoxin derivatives with selectivity for the $\alpha_2\beta_3$ isoform of Na,K-ATPase potently reduce intraocular pressure. *Proc. Natl. Acad. Sci. U.S.A.* **112**, 13723–13728
27. Katz, A., Tal, D. M., Heller, D., Haviv, H., Rabah, B., Barkana, Y., Marcovich, A. L., and Karlish, S. J. (2014) Digoxin derivatives with enhanced selectivity for the α_2 isoform of Na,K-ATPase: effects on intraocular pressure in rabbits. *J. Biol. Chem.* **289**, 21153–21162

28. Cirri, E., Katz, A., Mishra, N. K., Belogus, T., Lifshitz, Y., Garty, H., Karlish, S. J., and Apell, H. J. (2011) Phospholemman (FXYD1) raises the affinity of the human α1β1 isoform of Na,K-ATPase for Na ions. *Biochemistry* **50**, 3736–3748

29. Habeck, M., Haviv, H., Katz, A., Kapri-Pardes, E., Ayciriex, S., Shevchenko, A., Ogawa, H., Toyoshima, C., and Karlish, S. J. (2015) Stimulation, inhibition, or stabilization of Na,K-ATPase caused by specific lipid interactions at distinct sites. *J. Biol. Chem.* **290**, 4829–4842

30. Mishra, N. K., Habeck, M., Kirchner, C., Haviv, H., Peleg, Y., Eisenstein, M., Apell, H. J., and Karlish, S. J. (2015) Molecular mechanisms and kinetic effects of FXYD1 and phosphomimetic mutants on purified human Na,K-ATPase. *J. Biol. Chem.* **290**, 28746–28759

31. Wasserstrom, J. A., and Aistrup, G. L. (2005) Digitalis: new actions for an old drug. *Am. J. Physiol. Heart Circ. Physiol.* **289**, H1781–H1793

32. Schwinger, R. H., Bundgaard, H., Müller-Ehmsen, J., and Kjeldsen, K. (2003) The Na,K-ATPase in the failing human heart. *Cardiovasc. Res.* **57**, 913–920

33. André, N., Cherouati, N., Prual, C., Steffan, T., Zeder-Lutz, G., Magnin, T., Pattus, F., Michel, H., Wagner, R., and Reinhart, C. (2006) Enhancing functional production of G protein-coupled receptors in *Pichia pastoris* to levels required for structural studies via a single expression screen. *Protein Sci.* **15**, 1115–1126

34. Cohen, E., Goldshleger, R., Shainskaya, A., Tal, D. M., Ebel, C., le Maire, M., and Karlish, S. J. (2005) Purification of Na$^+$,K$^+$-ATPase expressed in *Pichia pastoris* reveals an essential role of phospholipid-protein interactions. *J. Biol. Chem.* **280**, 16610–16618

35. Lifshitz, Y., Petrovich, E., Haviv, H., Goldshleger, R., Tal, D. M., Garty, H., and Karlish, S. J. (2007) Purification of the human α2 Isoform of Na,K-ATPase expressed in *Pichia pastoris*: stabilization by lipids and FXYD1. *Biochemistry* **46**, 14937–14950

36. Cantley, L. C., Jr., Cantley, L. G., and Josephson, L. (1978) A characterization of vanadate interactions with the (Na,K)-ATPase: mechanistic and regulatory implications. *J. Biol. Chem.* **253**, 7361–7368

37. Habeck, M., Cirri, E., Katz, A., Karlish, S. J., and Apell, H. J. (2009) Investigation of electrogenic partial reactions in detergent-solubilized Na,K-ATPase. *Biochemistry* **48**, 9147–9155

38. Forbush, B. (1983) Cardiotonic steroid binding to Na,K-ATPase. *Curr. Top. Membr. Transp.* **19**, 167–201

39. Gloor, S., Antonicek, H., Sweadner, K. J., Pagliusi, S., Frank, R., Moos, M., and Schachner, M. (1990) The adhesion molecule on glia (AMOG) is a homologue of the β subunit of the Na,K-ATPase. *J. Cell Biol.* **110**, 165–174

40. Bossuyt, J., Despa, S., Han, F., Hou, Z., Robia, S. L., Lingrel, J. B., and Bers, D. M. (2009) Isoform specificity of the Na/K-ATPase association and regulation by phospholemman. *J. Biol. Chem.* **284**, 26749–26757

41. Vagin, O., Turdikulova, S., and Tokhtaeva, E. (2007) Polarized membrane distribution of potassium-dependent ion pumps in epithelial cells: different roles of the *N*-glycans of their β subunits. *Cell Biochem. Biophys.* **47**, 376–391

42. Vagin, O., Sachs, G., and Tokhtaeva, E. (2007) The roles of the Na,K-ATPase β1 subunit in pump sorting and epithelial integrity. *J. Bioenerg. Biomembr.* **39**, 367–372

43. Antonicek, H., Persohn, E., and Schachner, M. (1987) Biochemical and functional characterization of a novel neuron-glia adhesion molecule that is involved in neuronal migration. *J. Cell Biol.* **104**, 1587–1595

44. Schmalzing, G., Kröner, S., Schachner, M., and Gloor, S. (1992) The adhesion molecule on glia (AMOG/β2) and α1 subunits assemble to functional sodium pumps in *Xenopus* oocytes. *J. Biol. Chem.* **267**, 20212–20216

45. Eakle, K. A., Kabalin, M. A., Wang, S. G., and Farley, R. A. (1994) The influence of beta subunit structure on the stability of Na$^+$/K$^+$-ATPase complexes and interaction with K$^+$. *J. Biol. Chem.* **269**, 6550–6557

46. Colonna, T. E., Huynh, L., and Fambrough, D. M. (1997) Subunit interactions in the Na,K-ATPase explored with the yeast two-hybrid system. *J. Biol. Chem.* **272**, 12366–12372

47. Lutsenko, S., and Kaplan, J. H. (1993) An essential role for the extracellular domain of the Na,K-ATPase β-subunit in cation occlusion. *Biochemistry* **32**, 6737–6743

48. Morth, J. P., Pedersen, B. P., Toustrup-Jensen, M. S., Sørensen, T. L., Petersen, J., Andersen, J. P., Vilsen, B., and Nissen, P. (2007) Crystal structure of the sodium-potassium pump. *Nature* **450**, 1043–1049

49. Shinoda, T., Ogawa, H., Cornelius, F., and Toyoshima, C. (2009) Crystal structure of the sodium-potassium pump at 2.4 Å resolution. *Nature* **459**, 446–450

50. Kanai, R., Ogawa, H., Vilsen, B., Cornelius, F., and Toyoshima, C. (2013) Crystal structure of a Na$^+$-bound Na$^+$,K$^+$-ATPase preceding the E1P state. *Nature* **502**, 201–206

51. Laursen, M., Gregersen, J. L., Yatime, L., Nissen, P., and Fedosova, N. U. (2015) Structures and characterization of digoxin- and bufalin-bound Na$^+$,K$^+$-ATPase compared with the ouabain-bound complex. *Proc. Natl. Acad. Sci. U.S.A.* **112**, 1755–1760

52. Larsen, B. R., Assentoft, M., Cotrina, M. L., Hua, S. Z., Nedergaard, M., Kaila, K., Voipio, J., and MacAulay, N. (2014) Contributions of the Na$^+$/K$^+$-ATPase, NKCC1, and Kir4.1 to hippocampal K$^+$ clearance and volume responses. *Glia* **62**, 608–622

53. DiFranco, M., Hakimjavadi, H., Lingrel, J. B., and Heiny, J. A. (2015) Na,K-ATPase α2 activity in mammalian skeletal muscle T-tubules is acutely stimulated by extracellular K$^+$. *J. Gen. Physiol.* **146**, 281–294

54. Clausen, T. (2008) Regulatory role of translocation of Na$^+$-K$^+$ pumps in skeletal muscle: hypothesis or reality? *Am. J. Physiol. Endocrinol. Metab.* **295**, E727–E728; author reply 729

55. Correll, R. N., Eder, P., Burr, A. R., Despa, S., Davis, J., Bers, D. M., and Molkentin, J. D. (2014) Overexpression of the Na$^+$/K$^+$ ATPase α2 but not α1 isoform attenuates pathological cardiac hypertrophy and remodeling. *Circ. Res.* **114**, 249–256

56. Yang, E. H., Shah, S., and Criley, J. M. (2012) Digitalis toxicity: a fading but crucial complication to recognize. *Am. J. Med.* **125**, 337–343

57. Chan, K. E., Lazarus, J. M., and Hakim, R. M. (2010) Digoxin associates with mortality in ESRD. *J. Am. Soc. Nephrol.* **21**, 1550–1559

58. Hoffman, B. K., and Bigger, J. T. (1985) Digitalis and allied cardiac glycosides. in *The Pharmacological Basis of Therapeutics*, 7th Ed. (Goodman, A., Gilman, L. S., Rall, T. W., and Murad, F., eds) pp. 716–747, Macmillan, New York

59. Bagrov, A. Y., Shapiro, J. I., and Fedorova, O. V. (2009) Endogenous cardiotonic steroids: physiology, pharmacology, and novel therapeutic targets. *Pharmacol. Rev.* **61**, 9–38

60. Blaustein, M. P., Zhang, J., Chen, L., Song, H., Raina, H., Kinsey, S. P., Izuka, M., Iwamoto, T., Kotlikoff, M. I., Lingrel, J. B., Philipson, K. D., Wier, W. G., and Hamlyn, J. M. (2009) The pump, the exchanger, and endogenous ouabain: signaling mechanisms that link salt retention to hypertension. *Hypertension* **53**, 291–298

61. Lingrel, J. B. (2010) The physiological significance of the cardiotonic steroid/ouabain-binding site of the Na,K-ATPase. *Annu. Rev. Physiol.* **72**, 395–412

62. Rindler, T. N., Dostanic, I., Lasko, V. M., Nieman, M. L., Neumann, J. C., Lorenz, J. N., and Lingrel, J. B. (2011) Knockout of the Na,K-ATPase α_2-isoform in the cardiovascular system does not alter basal blood pressure but prevents ACTH-induced hypertension. *Am. J. Physiol. Heart Circ. Physiol.* **301**, H1396–H1404

63. Loreaux, E. L., Kaul, B., Lorenz, J. N., and Lingrel, J. B. (2008) Ouabain-Sensitive α1 Na,K-ATPase enhances natriuretic response to saline load. *J. Am. Soc. Nephrol.* **19**, 1947–1954

64. Gatto, C., Wang, A. X., and Kaplan, J. H. (1998) The M4M5 cytoplasmic loop of the Na,K-ATPase, overexpressed in *Escherichia coli*, binds nucleoside triphosphates with the same selectivity as the intact native protein. *J. Biol. Chem.* **273**, 10578–10585

65. Tokhtaeva, E., Sachs, G., and Vagin, O. (2010) Diverse pathways for maturation of the Na,K-ATPase β1 and β2 subunits in the endoplasmic reticulum of Madin-Darby canine kidney cells. *J. Biol. Chem.* **285**, 39289–39302

66. Strugatsky, D., Gottschalk, K. E., Goldshleger, R., Bibi, E., and Karlish, S. J. (2003) Expression of Na$^+$,K$^+$-ATPase in *Pichia pastoris*: analysis of wild type and D369N mutant proteins by Fe^{2+}-catalyzed oxidative cleavage and molecular modeling. *J. Biol. Chem.* **278**, 46064–46073

67. Mishra, N. K., Peleg, Y., Cirri, E., Belogus, T., Lifshitz, Y., Voelker, D. R., Apell, H. J., Garty, H., and Karlish, S. J. (2011) FXYD proteins stabilize

Na,K-ATPase: amplification of specific phosphatidylserine-protein interactions. *J. Biol. Chem.* **286,** 9699 –9712

68. Crambert, G., Fuzesi, M., Garty, H., Karlish, S., and Geering, K. (2002) Phospholemman (FXYD1) associates with Na,K-ATPase and regulates its transport properties. *Proc. Natl. Acad. Sci. U.S.A.* **99,** 11476 –11481

69. Haviv, H., Cohen, E., Lifshitz, Y., Tal, D. M., Goldshleger, R., and Karlish, S. J. (2007) Stabilization of Na$^+$,K$^+$-ATPase purified from *Pichia pastoris* membranes by specific interactions with lipids. *Biochemistry* **46,** 12855 –12867

70. Haviv, H., Habeck, M., Kanai, R., Toyoshima, C., and Karlish, S. J. (2013) Neutral phospholipids stimulate Na,K-ATPase activity: a specific lipid-protein interaction. *J. Biol. Chem.* **288,** 10073 –10081

71. Kapri-Pardes, E., Katz, A., Haviv, H., Mahmmoud, Y., Ilan, M., Khalfin-Penigel, I., Carmeli, S., Yarden, O., and Karlish, S. J. (2011) Stabilization of the α2 isoform of Na,K-ATPase by mutations in a phospholipid binding pocket. *J. Biol. Chem.* **286,** 42888 – 42899

72. Bowie, J. U., Lüthy, R., and Eisenberg, D. (1991) A method to identify protein sequences that fold into a known three-dimensional structure. *Science* **253,** 164 –170

73. Lovell, S. C., Davis, I. W., Arendall, W. B., 3rd, de Bakker, P. I., Word, J. M., Prisant, M. G., Richardson, J. S., and Richardson, D. C. (2003) Structure validation by Calpha geometry: ϕ,ψ and Cβ deviation. *Proteins* **50,** 437– 450

74. Brooks, B. R., Brooks, C. L., 3rd, Mackerell, A. D., Jr., Nilsson, L., Petrella, R. J., Roux, B., Won, Y., Archontis, G., Bartels, C., Boresch, S., Caflisch, A., Caves, L., Cui, Q., Dinner, A. R., Feig, M., *et al.* (2009) CHARMM: the biomolecular simulation program. *J. Comput. Chem.* **30,** 1545–1614

75. Wu, G., Robertson, D. H., Brooks, C. L., 3rd, and Vieth, M. (2003) Detailed analysis of grid-based molecular docking: a case study of CDOCKER-A CHARMm-based MD docking algorithm. *J. Comput. Chem.* **24,** 1549 –1562

76. Tal, D. M., Karlish, S. J., and Gottlieb, H. E. (2016) An NMR study of new cardiac glycoside derivatives. *Magn. Reson. Chem.* **54,** 260 –262